Plasmoids and the E-to-H transition in an Inductively Coupled Plasma

A thesis for the degree of

PHILOSOPHIAE DOCTOR

Presented to

DUBLIN CITY UNIVERSITY

By

ANGUS J MCCARTER MSci.
School of Physical Sciences
Dublin City University

Research Supervisors

Dr Michael B Hopkins and

Prof. Miles M. Turner

External Examiner Prof W.G. Graham

Internal Examiner· Dr E. McGlynn

Dec 2005

Declaration

I hereby certify that this material which I now submit for assessment on the programme of study leading to the award of Philosophiae Doctor is entirely my own work and has not been taken from the work of others save and to the extent that such work has been cited and acknowledged within the text of this work.

Angus McCarter

Angus McCarter, Dec 2005

Dedicated to

Mum, Dad, Aeidin and Austin

And in memory of

May and Jimmy Purcell

and

Kathleen and Gerald McCarter

Abstract

An Inductively Coupled Plasma (ICP) exhibits two distinct modes of operation A low input power capacitive E-mode, and a high input power inductive H-mode The gas initially breaks down in the E-mode, switching to H-mode as input power is increased above a certain threshold This transition between the E and H modes is observed by a dramatic increase in light output from the plasma, and a 'glitch' in the antenna current as the load characteristics of the plasma change from capacitive to inductive The transition between the E and H modes exhibits hysteresis

The effect of introducing small amounts of molecular oxygen in an argon plasma on the E-to-H transition has been investigated It has been observed that the addition of small amounts of molecular gas increases the size of the hysteresis instability window in the system, and also increases the ignition current required for the inductive mode

Within the E-to-H instability window, gross spatial inhomogeneities (plasmoids) have been observed We report the observation of plasmoids in a cylindrical inductively coupled rf plasma Observations show plasmoid lobes as regions of higher plasma density and light emission distributed symmetrically around the antenna They may also rotate and the number of lobes may change depending of plasma power, pressure, and gas mixture

In order to explain the behaviour of plasmoids we present the discharge as plasma transmission line with associated line capacitance and inductance as defined by the plasma Plasmoids may be shown to be standing waves showing density and absorbed power modulation consistent with observed experimental results A plasma simulation coupled to the theoretical model also shows results consistent with experimental observation

Contents

List of Figures

LIST OF FIGURES

List of symbols

A	area (m^{-2})
V	plasma volume (m^3)
d	transmission line length (m)
D	diffusion coefficient (m^2s^{-1}), D_a ambipolar diffusion coefficient, drift energy flux (Wm^{-2})
e	absolute electron charge ($\simeq 1\,6 \times 10^{19}$ C)
E	electric field (Vm^{-1})
f	frequency (Hz)
I	current (A), I_{rf} antenna current (A)
J	current density (Am^{-2})
k	Boltzmann's constant ($\simeq 1\,381 \times 10^{-23}$ JK^{-1})
l	length (m)
m	mass (kg), m_e electron mass ($\simeq 9\,1 \times 10^{-31}$ kg), m_i ion mass

continued on next page

continued from previous page

n	particle number density (m^{-3}), n_e electron density, n_i ion density, n_g neutral gas density
P	power (W), P_{abs} absorbed power (W), P_{diss} dissipated power (W)
p	pressure (mTorr)
q	electric charge (C)
s	sheath width (m)
t	time (s)
T	temperature (K or Volts)
u_B	u_B Bohm velocity
v_e	average electron velocity
v_p	phase velocity (ms^{-1})
V	electric potential (V)
Γ	particle flux ($m^{-2}s^{-1}$)
δ	Skin Depth (m)
ϵ_0	vacuum permittivity ($\simeq 8\,8 \times 10^{-12}$ Fm^{-1})
μ_0	vacuum permeability ($\simeq 4\pi \times 10^{-7}$ Hm^{-1})
λ	mean free path (m), λ_i ion mean free path, λ_D electron Debye length (m)
μ	mobility ($m^2s^{-1}V^{-1}$), μ_e electron mobility, μ_i ion mobility
ν	collision frequency (Hz)
ν_{eff}	effective electron-neutral collision frequency (Hz)
σ	cross section (m^{-2}), electrical conductivity ($\Omega^{-1}m^{-1}$)
ϕ	angle (rad)

continued on next page

continued from previous page

Φ	potential (V)
ω	angular frequency (rad s^{-1}), ω_{pe} electron plasma frequency, ω_{pi} ion plasma frequency
Γ	diffusion length (m)

CHAPTER 1

Introduction

1.1 What is a plasma?

A plasma is a quasineutral (approximately equal numbers of positively and negatively charged particles) completely or partially ionised gas that exhibits collective behaviour The density and temperature of these particles can span over many orders of magnitude with plasma science usually classified into various disciplines according to the plasma density and temperature A log-log plot of density versus temperature (fig 1 1) gives an indication of the range of plasma disciplines Here we can see a sample of the many aspects of plasma science ranging from such diverse topics as electrical plasmas, nuclear fusion technology, astrophysics, gas lasers and space physics

Plasmas can be more comprehensively defined by using the plasma parameters of Debye length and plasma frequency

Debye Length

The ability of a plasma to screen out electric fields over a characteristic length known as the Debye length, is due to the greater mobility of electrons compared to the heavier ions In the presence of an electric field, negative electrons are accelerated away leaving a positive ion charge The resulting electric field retards the motion of electrons within a Debye sphere of radius the Debye length, λ_D In order to sustain a plasma discharge the discharge length, L, must be significantly greater than the Debye length This places the condition

$$L \gg \lambda_D \tag{1 1}$$

There must also be a significant number of electrons within the Debye sphere in order to constitute a plasma This places the additional condition

$$N_D \gg 1 \tag{1 2}$$

where N_D is the number of electrons contained within the Debye sphere

Plasma Frequency

When a disturbance is imposed on a collection of charged particles the particles response tends to create particle oscillations in the plasma The characteristic response frequency is known as the plasma frequency, ω_p and is the frequency with which charged particles respond to an external disturbance If a collection of charged particles are oscillating at the plasma frequency and some collisions with the background gas cause the oscillations to be damped, the plasma is said be an ionised gas as opposed to a plasma The final condition for an ionised gas to be considered a plasma, is that the charged particle - neutral gas collision frequency, ν_m, must be less than the plasma frequency

$$\nu_m < \omega_p \tag{1 3}$$

1.2 Motivation

This work is primarily concerned with electrically generated, and more specifically radio frequency, plasmas Radio frequency (rf) plasmas are generated by applying an rf electric field across a gas containing some residual electrons The electrons are accelerated causing collisions with the background gas Some of these collisions may lead to ionisation of the background gas generating more electrons and more collisions An avalanche effect takes place leading to plasma formation

Plasmas used for industrial processes are usually in the plasma density range of $10^{14}m^{-3}$ – $10^{18}m^{-3}$ and the electron temperature range of 2-5 eV These processes are primarily concerned with the etching or deposition of material onto a substrate There are countless types of processing plasma used in a myriad of different industries with the multi-billion dollar semiconductor industry being the most prominent of these A significant component of industrial plasma research is aimed at improving the processes used in semiconductor manufacturing There are many highly developed semiconductor plasma tools however the complexity of these devices means that the physics of these are poorly understood with a 'trial-and-error' approach used to improve the efficiency of a particular device and process In our experimental system we have a plasma discharge which is geometrically simple compared to industrial tools and is more easily characterised This enables us to build on the fundamental knowledge of plasmas without the complexity of an industrial device

On a more specific level, we use an argon discharge with molecular gas mixtures similar to those used in industrial style processes Research into this area allows us to better understand the plasma dynamics of argon mixtures that may be utilised in an industrial context Perhaps most importantly, we investigate the formation of gross spatial non-uniformities and propose a theory for their formation Non-uniform plasmas are detrimental to quality control of fabrication processes and any

further understanding of these is beneficial

1.3 Structure of the Thesis

The structure of this thesis is as follows In the introduction we give an overview of plasma physics in an industrial context and outline the motivation behind this work We will also introduce the relevant plasma physics required later in the thesis This is not intended as a general introduction to plasma physics, of which there are many excellent texts, but merely as an introduction and reference for the concepts and formulae required later Chapter 2 describes the experimental setup and relevant experimental information Chapter 3 deals with the E-to-H transition and the effect of molecular gas mixtures in an argon inductively coupled plasma (ICP) discharge The E-to-H transition is a well documented [3, 4, 5, 1] phenomenon in ICP discharges and concerns the power transfer mechanism between capacitive and inductive power coupling in an ICP The hysteresis 'window' in which both power transfer modes are available over a range of input power is studied both experimentally and using a global model Another well documented phenomenon is that of plasma instabilities [6, 7] observed within the hysteresis window - which we will now refer to as the instability window These instabilities range from high frequency ($\sim$ kHz) oscillations of light intensity and electron density to gross spatial inhomogeneities referred to as 'plasmoids' [8, 9, 10] Although attempts were made to observe the high frequency instabilities in our ICP system, none were observed However, we were able to readily observe plasmoids within the instability window Chapter 4 is an experimental characterisation of plasmoids observed in our ICP system The work recounts the work of Crowley [2] and further characterises the behaviour of plasmoids particularly in relation to plasmoid rotation In Chapter 5, a model is proposed to explain the formation of plasmoids The model considers the inductively coupled plasma as

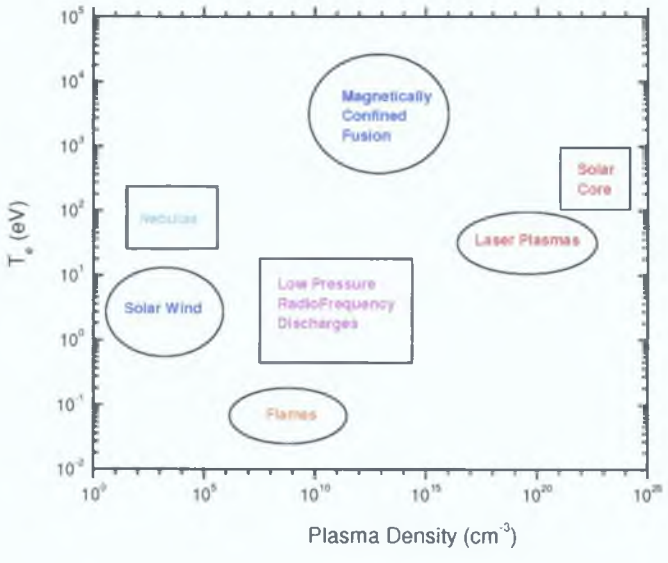

Figure 1.1: *Log-Log plot of plasma density versus temperature*

a transmission line with plasmoids modelled as standing waves. Chapter 6 extends the transmission line model to simulate plasmoids formation from a uniform plasma to plasma containing plasmoids. Finally in chapter 7, a summary and conclusion of the work is given with proposals for further work.

1.4 Plasma Physics and Industrial Plasmas

A plasma may be loosely defined as a partially or fully ionised gas containing approximately equal numbers of positively and negatively charged particles. Plasmas usually exhibit some type of collective behaviour that allows it to be characterised by certain properties such as plasma density, plasma temperature, Debye length and plasma frequency.

Industrial plasmas are generated in a variety of ways such as inductively coupled

plasmas, capacitively coupled plasmas, microwave sources and others The main application of these plasma devices is to use the plasma constituents (electrons, ions, atoms, molecules) to deposit material onto a substrate, etch material off a substrate or to do some type of surface modification The type of plasma device used depends on the plasma properties required for the plasma process Some of the desirable characteristics for plasma processing, particularly in relation to semiconductor manufacturing are

- High etch rate - Material is removed quickly and efficiently from a substrate to create the desired pattern
- Anisotropy - Energetic ions are required to preferentially etch in one direction leaving a straight trench wall perpendicular to the surface
- Uniformity - Deposited material onto a substrate is required to be evenly distributed which requires a uniform plasma
- Selectivity - During surface modification where a surface is made up of different materials, the plasma is required to process only one of the materials leaving the others unaffected

Some of the more common types of industrial discharge are outlined below

Reactive Ion Etch Discharges (RIE)

Reactive Ion Etch (RIE) Discharges are capacitively coupled devices where plasma is generated between two flat circular electrodes approximately 10cm apart The substrate to be processed is placed on the lower electrode which is usually grounded The upper electrode is driven by a voltage oscillating at the standard industrial operating frequency of 13 56 MHz Gas is fed into the vacuum discharge chamber

where residual electrons are accelerated by the oscillating electric field The accelerated electrons collide with the background gas causing ionisation and plasma formation The plasma is isolated from the electrodes and surrounding chamber walls by formation of the plasma sheath The positive plasma potential drives ions across the sheath onto the substrate and etches material from the substrate Independent control of the ion energy and flux impinging onto the surface may be controlled by biasing the lower electrode with either a DC or oscillating voltage

Inductively Coupled Plasmas (ICP)

Inductively coupled plasmas are generated using an antenna of some configuration usually driven at 13 56 MHz located near the discharge region The oscillating current in the antenna generates a magnetic field in accordance with Ampere's law, this oscillating magnetic field induces an electric field in the discharge region in accordance with Faraday's law The induced electric field accelerates residual electrons that collide with the background gas causing collisional ionisation and plasma formation There are various configurations of ICP discharge with the most common being the Transformer Coupled Plasma (TCP), the Helical Resonator, and the Detached Plasma Source (DPS) The TCP uses a 'stove top' flat spiral antenna placed at one end of a cylindrical discharge region with the processing substrate placed at the other The Helical Resonator uses an helical antenna wrapped around the discharge region In this device the antenna has an electrical length that resonates with the driving frequency, that allows the antenna current to oscillate back and forth along the antenna length thereby generating the inductive plasma The DPS system uses a combination of flat spiral and helical antenna configuration The antenna is shaped as if it has been wrapped around a dome with the feed gas placed inside the dome This has the advantage of placing the source region away from the substrate allowing the plasma to evolve via diffusion into a uniform plasma before

impinging onto the work piece

Helicon Discharges

Helicon Discharges are similar to ICP in that they use an antenna driven at radio frequencies to generate the plasma in the discharge region However Helicons, employ a magnetic field to increase the skin depth and allow the electromagnetic wave to penetrate fully into the plasma, it also confines electrons in the discharge region This has the advantage of generating a higher density plasma than that attainable by ICP methods

1.5 Introduction to Inductively Coupled Plasmas

Inductively coupled plasmas have been known and researched for well over one hundred years [11] with the recent boom in the microelectronics industry prompting a massive amount of research into ICP's and plasma physics in general Properties of ICP's include high densities of ions and electrons, low and controllable ion energies and plasma uniformity, all of which are requirements in many plasma processing techniques such as plasma etching, sputtering and deposition Although huge progress has been made in recent years, the demand for faster, more accurate, and more efficient process control ensures that plasma physics remains a highly active research field

Radio Frequency (rf) inductively coupled plasmas are generated using the principle of electromagnetic induction An inductive element (an antenna of some configuration) is driven by an rf current and positioned near the discharge region The rf current generates an rf magnetic field which in turn induces an rf electric field in the discharge region in accordance with Faraday's Law The induced electric field accelerates free electrons within the discharge causing ionisations and subsequently

plasma formation

Applications of ICP's include sputtering of metal targets with a particular gas (usually argon), etching microelectronic circuits onto a substrate, rf ion thrusters used to manoeuvre satellites etc

Inductively coupled plasmas transfer power from the rf power generator into the plasma by radiating electromagnetic energy from the antenna into the gas contained in the discharge chamber A typical inductive discharge plasma with electron density $\sim 10^{11} cm^{-3}$, has a plasma frequency of $\sim 2840 MHz$ (calculated approximately by $f_{pe} \simeq 8980\sqrt{n_e}$ where n_e is the plasma density in cm^{-3}) At this frequency the plasma is opaque to an em wave radiating at 13 56MHz and therefore only penetrates the plasma volume a finite distance known as the skin depth The skin depth defines the power deposition volume for the radiating em wave emitted from the antenna As the electromagnetic wave penetrates into the plasma volume, electrons are accelerated by the induced electric field The flow of electrons within the plasma is considered to be a current flowing in a conducting medium, and the power delivered to the plasma depends on its complex conductivity Before we discuss power deposition in an ICP it is instructive to detail the concepts of plasma skin depth and complex plasma conductivity which will be required in the discussion of power deposition

1 5 1 Complex Plasma Conductivity

It is necessary to introduce a complex conductivity (σ) for two reasons (a) to account for the fact that current carrying electrons within a plasma discharge under the influence of an RF electric field undergo collisions with the background gas, and (b) that the finite mass of electrons affects the electron's response to the electric field This introduces a phase between the applied rf voltage and current in the plasma We may quantify the complex conductivity by considering electrons in a

plasma under the influence of a sinusoidally varying electric field in the x-direction, $E_x(t) = Re[\bar{E}_x e^{\jmath\omega t}]$ assuming infinite ion mass [12] It is assumed that all time varying quantities vary sinusoidally with a frequency ω The usual procedure is to write the electron equation of motion

$$m\frac{du_x}{dt} = -eE_x - m\nu_m u_x \tag{1 4}$$

where the force term on the left hand side is balanced by the force of the electric field, E, acting on the electronic charge, e, and the frictional drag of the electrons due to electron-neutral collisions occurring with a collision frequency ν_m Considering electron velocity in the x-direction is varying sinusoidally, $u_x = Re[\bar{u}e^{\jmath wt}]$, then equation (1 4) may be written as

$$u = -\frac{e}{m}\frac{1}{\jmath\omega + \nu_m}E \tag{1 5}$$

We now relate the velocity of the electrons to the current density **J** by introducing the total current

$$J_{total} = \epsilon\frac{\partial E}{\partial t} + J_{conduction} \tag{1 6}$$

where $\epsilon\frac{\partial E}{\partial t}$ is the displacement current and $J_{conduction}$ is the conduction current due solely to electron motion

$$J_{conduction} = -en_0\bar{u}_x \tag{1 7}$$

we also have

$$\frac{\partial E_x}{\partial t} = Re\jmath\omega\bar{E}_x e^{\jmath\omega t} \tag{1 8}$$

we may now write J_{total} as

$$J_{total} = \jmath\omega\epsilon_0\bar{E}_x - en_0\bar{u}_x \tag{1 9}$$

Using (1 5) and (1 9) we obtain

$$J_{total} = \jmath\omega\epsilon_0\left[1 - \frac{\omega_{pe}^2}{\omega(\omega - \jmath\nu_m)}\right]E \tag{1 10}$$

where $\omega_{pe}^2 = \frac{e^2 n_e}{\epsilon_0 m}$ is the plasma frequency Equation 1 10 relates the total current to the electric field, hence we may introduce an effective plasma dielectric constant

$$\epsilon = \epsilon_0 \kappa_p = \epsilon \left[1 - \frac{\omega_{pe}^2}{\omega(\omega - j\nu_m)} \right] E \tag{1 11}$$

where κ_p is the relative dielectric constant We may also introduce the complex plasma conductivity by writing (1 10) in the form $J_{total} = (\sigma + j\omega\epsilon_0)E$, with

$$\sigma = \frac{\epsilon_0 \omega_{pe}^2}{j\omega + \nu_m} \tag{1 12}$$

where σ is the complex plasma conductivity

1 5 2 Skin Depth

We will now consider the skin depth δ Evaluation of the skin depth requires analysis of the penetration of an electromagnetic wave emanating from the RF antenna into the plasma discharge characterised by a relative dielectric constant κ_p It can be shown using Maxwell's equations that an electromagnetic wave travelling in the x-direction may be characterised by

$$\frac{d^2 E_z}{dx^2} = -\frac{\omega^2}{c^2} \kappa_p E_z \tag{1 13}$$

where E_z is the electric field in the z-direction For an electromagnetic wave incident on a plasma boundary where the plasma is characterised by κ_P, it can be shown [13] that the em wave decays exponentially into the plasma with a decay constant

$$\alpha = \frac{\omega}{c} Im \kappa_p^{1/2} \equiv \frac{1}{\delta} \tag{1 14}$$

where

$$\kappa_p = 1 - \frac{\omega_{pe}^2}{\omega^2 (1 - j\nu_m/\omega)} \tag{1 15}$$

and δ is the skin depth and the plasma frequency $\omega_{pe} = (\frac{e^2 n_e}{\epsilon_0 m})^{1/2}$ There are two collisionality regimes

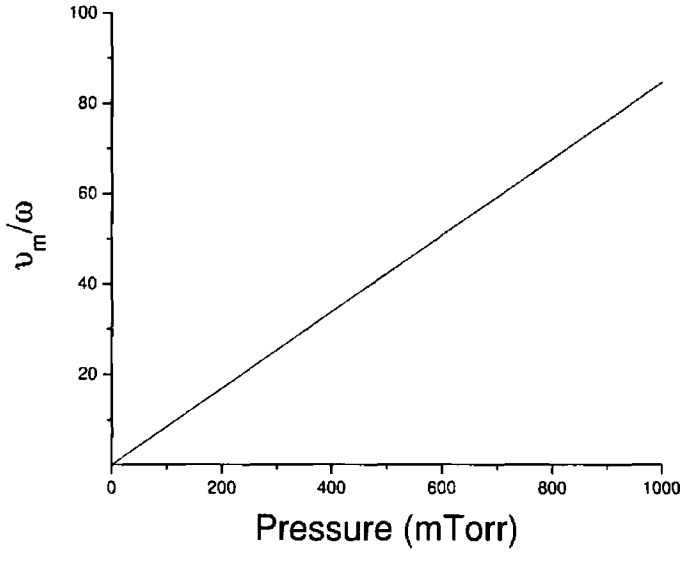

Figure 1 2 *ν_m/ω as a function of gas pressure*

For $\nu_m \ll \omega$, collisionless regime, ν_m/ω is neglected from (1 15) yielding

$$\delta_p = \left(\frac{m}{e^2\mu_0 n_s}\right)^{1/2} \tag{1 16}$$

For $\nu_m \gg \omega$, collisional regime, the 1 is dropped from the parenthesis of (1 15) yielding

$$\delta_c = \left(\frac{2m\nu_m}{\omega\mu_0 e^2 n_s}\right)^{1/2} \tag{1 17}$$

The majority of work carried out in this thesis where the skin depth is required is at gas pressures greater that > 50 mTorr, hence we use the collisional skin depth (equation 1 17) since $\nu_m \gg \omega$ (figure 1 2)

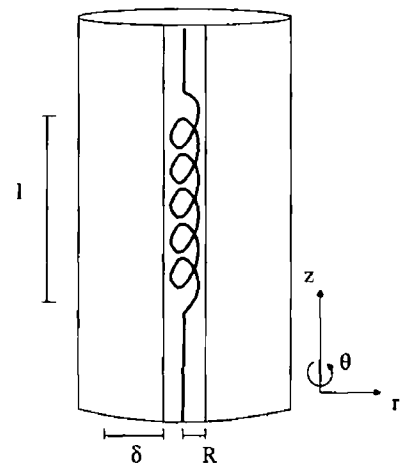

Figure 1 3 *Schematic representation of the ICP cylinder*

1 5.3 Power Deposition

Coupling of radio frequency (rf) electromagnetic energy is of primary interest when studying ICP discharges For the purposes of this work we detail the mechanisms whereby power is absorbed by the plasma from a radiating antenna The standard method in which to study this is through the so called transformer formalism as detailed by Piejak *et al* [14] In this work the plasma is considered to be a one-turn secondary of an air-core transformer where the antenna is the primary coil Power absorbed by the plasma from the antenna is considered in terms of the primary antenna current, the relevant inductances between the primary and secondary of the transformer, and the plasma density

Analysis begins by considering the power deposited into the plasma as given by

$$P_{abs} = \frac{1}{2}\int \mathbf{J}\ \mathbf{E}dV \tag{1 18}$$

where **J** is the current density vector in the plasma, **E** is the electric field vector in the plasma, and dV is the elemental volume into which power is absorbed (see fig 1 3) Assuming a cylindrical discharge of length l, radius of the dielectric tube R,

and $R \ll \delta$, the integral above evaluates to give

$$P_{abs} = \frac{1}{2}\mathbf{J} \quad \mathbf{E}2\pi(R+\delta)l\delta \tag{1 19}$$

Using Ohm's law, $J = \sigma E$, where σ is the plasma conductivity, 1 19 becomes

$$P_{abs} = \frac{1}{2}\frac{J_\theta^2}{\sigma}2\pi(R+\delta)l\delta \tag{1 20}$$

Where J_θ is the amplitude of the azimuthal current density in the plasma The plasma resistance maybe obtained by letting $J_\theta = I_p/l\delta$ and $P_{abs} = \frac{1}{2}I_p^2 R_p$ and combining with 1 20 to yield

$$R_p = \frac{2\pi(R+\delta)}{l\delta\sigma} \tag{1 21}$$

As well as a plasma resistance, the discharge also has an inductance associated with it [14] This inductance is made up of two components, the first is the geometrical inductance arising from the plasma considered to be a one-turn secondary of an air-core transformer, the second is the inductance arising from the electron inertia causing electrons to overshoot the oscillating electric field giving a phase lag between plasma current and electric field which may be considered to be an inductance The geometrical inductance L_p may be found by letting $L_p = \Phi/I_p$, with $\Phi = \mu_0 H_z A$, where A is the area threaded by the magnetic field H_z yielding

$$L_p = \frac{\mu_0 H_z A}{J_\theta l\delta} \tag{1 22}$$

The magnetic field due to current through area $A = \pi\delta(2r+\delta)$ is obtained using Ampere's law giving $H_z = J_\theta\delta$ This leads to an expression for plasma inductance

$$L_p = \frac{\mu_0\pi\delta(2r+\delta)}{l} \tag{1 23}$$

The electron inertia inductance may be calculated using the generalised form of Ohm's law and the complex plasma conductivity and considering that the current-voltage relation in an inductive circuit is $V = I_p(R_p + j\omega L_p)$

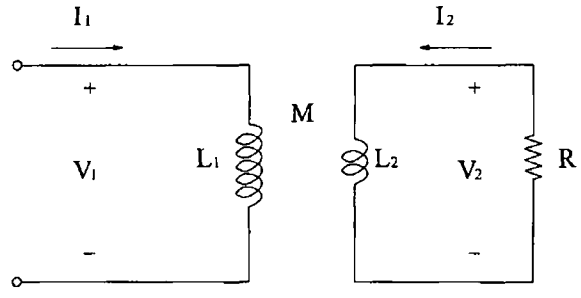

Figure 1 4 *Transformer Model*

The voltage V, is the integral of the azimuthal electric field E_θ around the current path i e $V = 2\pi\delta E_\theta$ The current I_p in terms of J_θ is $I_p = J_\theta l\delta$ Substituting into the generalised form of Ohm's law

$$J_\theta = \sigma_p E_\theta \tag{1 24}$$

where σ_p is the complex plasma conductivity given by equation (1 12), we may obtain an expression for the plasma inductance given by

$$L_p = \frac{R_p}{\nu_{eff}} \tag{1 25}$$

The preceding expressions detail the plasma resistance and inductance in terms of plasma current We now wish to use transformer formalism to obtain equivalent expressions in terms of antenna current

1.5.4 Transformer Formalism

Standard analysis of inductively coupled plasmas is to consider the plasma to be a one-turn secondary of an air-core transformer where the antenna is the primary winding If we consider an ideal transformer consisting of a primary winding (the antenna) with an inductance L_1, and a one turn secondary (the plasma) consisting

of an inductance L_2 and resistance R_2 They are coupled together by a mutual inductance M The standard technique [14] is to obtain the impedance, Z_A, as seen by the antenna due to the antenna impedance and the plasma impedance Considering the transformer in fig1 4, the primary circuit and secondary circuits may be described using Kirchhoff's voltage law

$$V_1 = L_1\frac{dI_1}{dt} - M\frac{dI_2}{dt} \tag{1 26}$$

$$V_2 = L_2\frac{dI_2}{dt} + I_2R_2 \tag{1 27}$$

The voltage induced in the secondary circuit,V_2, may be written as $V_2 = MdI_1/dt$ and dI/dt may be rewritten as $\jmath\omega I$ where ω is the angular driving frequency Equations 1 26 and 1 27 now become

$$V_1 = \jmath\omega L_1 I_1 - \jmath\omega M I_2 \tag{1 28}$$

$$\jmath\omega M I_1 = \jmath\omega L_2 I_2 + I_2 R_2 \tag{1 29}$$

Isolating I_2 in 1 29, inserting into 1 28, and rearranging to find V_1/I_1 gives the impedance Z_s

$$Z_s = \jmath\omega L_1 + \frac{(\omega M)^2}{R_2 + \jmath\omega L_2} \tag{1 30}$$

The resistance, R_s, and inductance, L_s, may be obtained by separating the real and imaginary components of Z_s Subsequently the resistance and inductance are

$$R_s = \frac{R_2(\omega M)^2}{R_2^2 - (\omega L_2)^2} \tag{1 31}$$

$$L_s = L_1 + \frac{(\omega M)^2 L_2}{R_2^2 - (\omega L_2)^2} \tag{1 32}$$

Using the assumption that $R_2^2 \ll \omega^2 L_2^2$ [13], (1 31) may be rewritten as

$$R_s = \frac{R_2(\omega M)^2}{(\omega L_2)^2} \tag{1 33}$$

1.5.5 Capacitive Coupling

In all inductively coupled systems, the antenna used the generate the inductive electric field can have a voltage of the order of kilovolts Inevitably there will be some capacitive power coupling into the plasma between the high voltage antenna and the grounded discharge chamber The effects of capacitive coupling may be reduced by inserting a Faraday shield between the antenna and the discharge chamber This is simply a thin grounded conducting sheath placed around the antenna with slits cut perpendicular to the antenna current flow to allow the magnetic field to penetrate the shield while grounding the capacitive voltage preventing penetration into the discharge region Although capacitive coupling may be undesirable, in many cases its ability to breakdown a gas to produce a plasma at low density is necessary to create enough electrons to attain the inductive mode Consideration of capacitive coupling is necessary in order to explain the well known E-to-H transition which will be detailed later

CHAPTER 2

Experimental Setup

BAsic Radiofrequency Inductive System (BARIS)

The BARIS discharge chamber consists of a helical antenna centered co-axially inside a cylindrical stainless steel discharge chamber (figure 2 1) The antenna is isolated from the discharge inside a quartz dielectric tube using a re-entrant configuration The antenna is driven at 13 56 MHz and is impedance matched to the rf generator using a standard 'L' configuration automatic matching unit In the following sections, a detailed description of the experimental setup is given

Discharge Chamber

The discharge chamber is a stainless steel cylindrical vacuum chamber of internal diameter 200mm and length 900mm (figure 2 2) One end of the chamber is sealed using a stainless steel flange which has a 50mm diameter port allowing a quartz tube

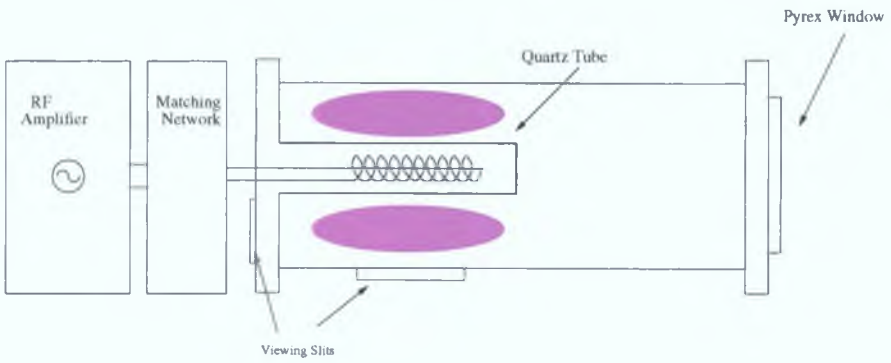

Figure 2.1: *A basic schematic of the BARIS Inductively Coupled Plasma system*

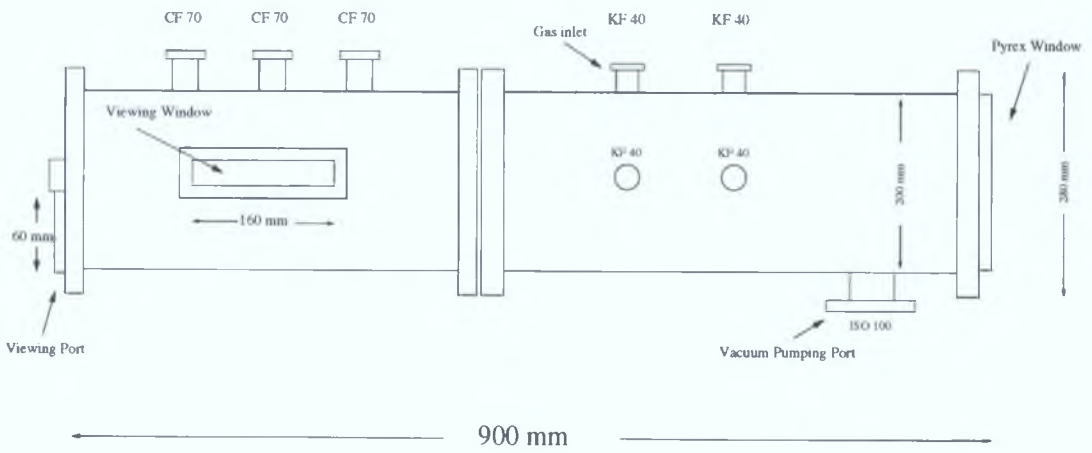

Figure 2.2: *A side view schematic of the BARIS discharge chamber*

to be inserted This configuration allows the antenna to be inserted into the body of the discharge region, while remaining outside the vacuum chamber This is known as a re-entrant configuration This end of the chamber also has a 20mm wide window extending from the edge of the antenna insertion point 60mm radially outwards towards the flange edge This slit was constructed to allow optical diagnostics to be used Another window, 25mm wide and 160mm long, was constructed into the chamber along the axial direction of the discharge chamber The other end of the chamber is sealed with a 15mm thick pyrex viewing window The discharge chamber is in two sections One section contains the antenna housing, the optical diagnostic windows and three conflat 70 vacuum ports for electrical diagnostics The second section contains a 100mm pumping port for the vacuum pumps and a KF 25 port for the gas inlet Various KF 25 ports are also available in the second section for needle valves and pressure gauges as required

Radio Frequency Generator

The radio frequency power supply was Marconi ACG-3 rf power supply operating at the standard industrial frequency of 13 56 MHz capable of delivering 300 Watts continuous power The rf power was monitored using two Bird 43 Thruline Wattmeters, one for forward power and one for reflected power

Matching Unit

The rf power is impedance matched to the plasma load using a standard 'L' configuration RFPP AM20 automatic matching unit (figure 2 3) The purpose of the matching unit is ensure maximum power transfer by impedance matching the rf source impedance R_s with the plasma discharge impedance $Z_{dischcarge}$ Since plasma impedance is a dynamic quantity, a variable matching unit must be used The standard 'L' configuration matchbox consists of a variable load capacitor C_L in parallel

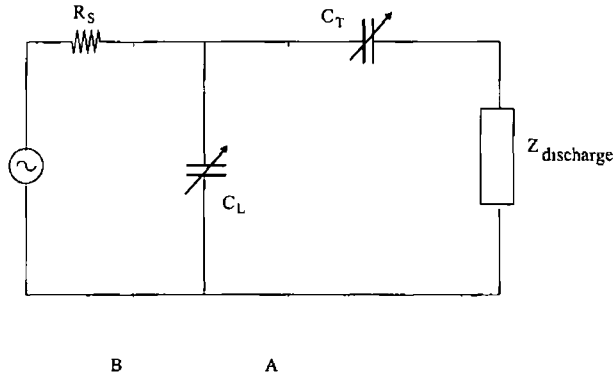

Figure 2 3 *Standard 'L' configuration matching unit consisting of a load capacitor (C_L) and a tune capacitor (C_T) matching a source impedance(R_S) to a plasma load impedance ($Z_{discharge}$)*

with the discharge, and a variable tune capacitor C_T in series with the discharge

The usual procedure to obtain matching conditions is to consider the impedance of the circuit as viewed at point A in figure 2 3, containing both $Z_{discharge}$ and the reactance of the tune capacitor $X_{CT} = -\frac{1}{\omega C_T}$ The impedance Z_A at point A is given by

$$Z_A = Z_{discharge} + jX_{CT} \tag{2 1}$$

We now consider the impedance as viewed at point B in figure 2 3 Since we now have an impedance Z_A in parallel with the reactance of the load capacitor $X_{CL} = -\frac{1}{\omega C_L}$, we can write the impedance Z_B as

$$Z_B = \frac{(Z_A)(jX_{CL})}{Z_A + jX_{CL}} \tag{2 2}$$

Maximum power transfer will occur when the resistive part of Z_B is equal to the source impedance, R_s, and the reactive part of Z_B is zero We can therefore determine the values of C_T and C_L for maximum power transfer by setting $Re(Z_B) = R_s$ and $Im(Z_B) = 0$

Antenna

The rf antenna was an 11 turn helical antenna with diameter 3 cm made out of a gold plated copper tube Water or compressed nitrogen was pumped through the antenna for cooling The antenna was centered co-axially inside a cylindrical stainless steel discharge chamber The antenna is isolated from the discharge inside a quartz dielectric tube using a re-entrant configuration [15]

Mass Flow Controllers

Gas flow was controlled using two STEC SEC-4000 Series Mass Flow Controllers (MFC) The MFC's employed a thermal sensor to measure the thermal conductivity of the gas and hence the flow rate The MFC's were calibrated for the particular gas in use and were capable of delivering 200 sccm's for argon and oxygen

Maintaining Vacuum

The base pressure was maintained at 10^{-7} mbar using an Edwards rotary pump and a Pfeiffer Balzers turbomolecular pump Pressure was monitored using a Baratron manometer gauge and an Inficon hot ion combi gauge

Probe Diagnostics

The primary diagnostic was a Scientific Systems® Plasma Impedance Monitor ™ (PIM) This device consisted of a current and voltage monitor located on the driven leg of the antenna The output from the PIM was fed into a Scientific Systems® PIM box which was externally controlled via computer

Optical Diagnostics

The optical diagnostics consisted of a Hamamatsu Photo Multiplier Tube (PMT) fed into a high frequency amplifier This device was used to monitor light fluctuation from the plasma

Phase Resolved Optical Emission Spectroscopy Setup

The phase resolved optical emission spectroscopy (PROES) is based on an Ocean Optics 200 μm optical fiber used to transfer emission from the BARIS discharge chamber to the PROES The PROES setup consists of a 1 5m Spectrometer allowing picometer wavelength resolution of the emitted radiation The spectrometer system is connected to an intensified charge coupled device (ICCD) capable of 5ns phase resolution

2.1 Experimental Method

The main experiments carried out in this work were the measurement of antenna current at the E-to-H transition points under varying conditions of gas pressure and gas composition The antenna current was measured using a Scientific Systems PIM^{TM} located between the matching unit and the rf antenna The plasma chamber was filled with argon or argon/oxygen mixtures to the desired pressure using the mass flow controllers or by adjusting the primary gate valve located on the underside of the chamber The pressure was varied over a pressure range from 10 to 1000 mTorr and gas composition varied from 100% argon to argon discharges containing up to 10% oxygen By varying the rf power from the rf signal generator/amplifier from minimum to maximum (0 - 300 Watts) and returning, the transition points for the E-to-H and H-to-E could be observed as a 'glitch' on the antenna current as measured by the PIM During all experiments presented in this work the matching

unit was switched to manual mode and the discharge was power 'matched' just before the E-to-H transition point and at the lowest pressure of 10mTorr Experiments to investigate the significance of the matching unit found no significant change in results depending on whether or not the matching unit was in automatic mode or 'matched' differently The main reason for maintaining the matching conditions described above were to obtain the maximum range of pressure in which a plasma could be maintained

During the plasmoid experiments the same procedure was employed In this case the power was varied from minimum to maximum and back and the antenna current for each number of plasmoids was noted

CHAPTER 3

E-to-H transition

In the following chapter we introduce the E-to-H mode transition and outline its present understanding We then detail the experimental results of the E-to-H transition in a pure argon ICP and in argon/oxygen mixtures as a function of pressure We then introduce an argon global model that shows good agreement with the experimental results Finally a short outline of an electromagnetic model is given for completeness

ICPs exhibit two distinct modes of operation [16] An E-mode, where rf power is deposited capacitively into the plasma discharge, and a H-mode, where rf power is deposited inductively into the plasma discharge

A common observation in ICPs is a mode jump from the low input power capacitive mode (E-mode) to the high input power inductive mode (H-mode) This E-to-H transition is observed on increasing input power to the antenna with a reverse H-to-E transition observed on decreasing input power The E-to-H transition is detected

by a dramatic increase in light output from the plasma and also by a 'glitch' in the antenna current as the load characteristics of the plasma change from capacitive to inductive The low power capacitive mode is due to electric fields between the high voltage antenna and the grounded discharge chamber These electric fields accelerate free electrons, creating a dimly lit plasma discharge characterised by a dim plasma glow and low electron density ($\sim 10^8 - 10^{10} cm^{-3}$) The inductive mode is due to the induced rf electric field, normally at right angles to the capacitive field in the plasma and has a brighter glow with higher electron density ($10^{10} - 10^{12} cm^{-3}$) It has been observed that the antenna current i_1 at which the E-to-H transition occurs, differs form the antenna current i_2 at which the reverse H-to-E transition occurs i e the transition exhibits hysteresis and there is a range of coil currents which may support both modes of operation depending on the history These effects arise from the various mechanisms involved in the power balance equation for an inductive discharge which we will discuss in more detail later

3.1 Power and Particle Balance

The following section is a discussion of power absorption and dissipation in ICPs as found in reference [1] Any stable plasma discharge must satisfy particle balance and power balance Particle balance states that the production of particles within the discharge volume must be offset by the loss of particles to the chamber walls

$$\int_v S dV = \int_s F dA \tag{3 1}$$

If we assume uniform plasma density (n_e) and electron temperature (T_e) then equation 3 1 may be re-written as

$$n_e u_B A_{eff} = K_{iz} n_g n_e \pi R^2 l \tag{3 2}$$

where the left hand side is the surface loss of particles through an effective plasma loss area A_{eff} with the Bohm velocity u_B The right hand side is the volume production of particles with the ionisation rate constant K_{iz}, times the gas density n_g, times the plasma volume $\pi R^2 l$ Rearranging equation 3 2 we obtain the familiar equation

$$\frac{K_{iz}(T_e)}{u_B(T_e)} = \frac{1}{n_g d_{eff}} \tag{3 3}$$

with d_{eff} representing *effective plasma size* Since the K_{iz} and u_B are known functions of electron temperature, then the electron temperature of the system may be determined from the gas density (pressure) and the discharge chamber dimensions [13]

The power balance equation states that power absorbed by the plasma electrons from the driven antenna (P_{abs}), must balance the power dissipated (P_{dis}) via electron collisions with other species throughout the plasma

$$P_{abs}(n_e) = P_{dis}(n_e) \tag{3 4}$$

A stable discharge will only exist when (3 1) and (3 4) are satisfied Initially we will treat a purely inductive discharge and describe how P_{abs} and P_{dis} vary with electron density There is no hysteresis in this treatment We will then introduce the various mechanisms associated with inductively coupled discharges which give rise to the hysteresis observed

In a purely inductive discharge, the power dissipated into the plasma volume is the power required to support an electron-ion pair over its lifetime If we assume that the electron temperature (T_e) is fixed, then the energy required to support an electron-ion pair over its lifetime (ε_{T_e}) is also fixed Therefore, P_{dis} is proportional to n_e i e as n_e increases, there are more electrons available to dissipate power, hence P_{dis} also increases The power dissipated by the plasma electrons may be written as [13]

$$P_{dis} = n_e u_B A_{eff} \varepsilon_{T_e} \tag{3.5}$$

where u_B is the Bohm velocity, A_{eff} is the effective surface area of the plasma and ε_{T_e} is the electron energy lost per electron-ion pair. We can see from (3.5) that the power dissipated varies linearly with electron density. The power absorbed may be estimated from the transformer model of an inductively coupled plasma, where the plasma discharge is considered to be the one-turn secondary of an air-core transformer[5, 14]. The RF current flows through the primary winding of the antenna which induces a current in the plasma secondary of the transformer system. The plasma has a geometrical inductance due the plasma acting as a closed conducting path around the antenna, an inductance due to electron inertia, and a resistance due to electron collisions within the discharge. Circuit analysis of the transformer model shows that the power absorbed by the plasma is related to the surface impedance of the plasma by

$$P_{abs} = \frac{1}{2} A_{plasma} Re Z I_{rf}^2 \tag{3.6}$$

where I_{rf} is the rf amplitude of the surface current in the plasma, Re[Z] is the real part of the complex plasma impedance and A_{plasma} is the surface area over which the plasma is excited [1].

The behaviour of P_{diss} and P_{abs} as a function of n_e is illustrated in figure 3.1. P_{diss} varies linearly with n_e as previously outlined. P_{abs} may be divided into two regimes, a low electron density regime and a high electron density regime. At low electron density, the induced field may be approximated as simply the vacuum field as found from Faraday's law, and the power absorbed scales a $P_{abs} \propto n_e$. As n_e increases, the skin depth becomes comparable to, and eventually smaller than, the dimensions of the discharge chamber. The skin effect now contains the penetration of the induced field to a small region inside the discharge chamber, restricting power

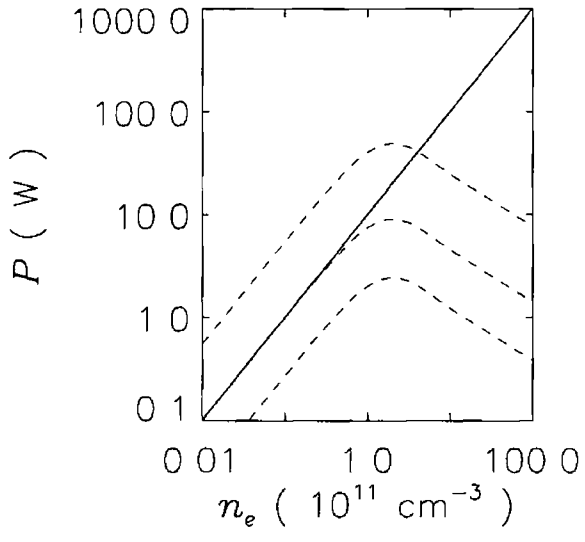

Figure 3 1 *P_{abs} (dashed line), P_{dis} (solid line) as a function of n_e in a purely inductive discharge The three dashed lines represent P_{abs} for an antenna current below the maintenance current required for an inductive discharge, an antenna current at the maintenance current, and an antenna current for a stable inductive mode No hysteresis is observed in this situation [1]*

deposition to the discharge volume inside the skin depth Since the skin depth is $\propto n^{-1/2}$ hence the power absorbed now scales as $P_{abs} \propto n_e^{-1/2}$ [13] The maximum power absorbed corresponds to a skin depth equivalent to the discharge dimensions Absorbed power is illustrated in figure 3 1 for three values of antenna current As can be seen, there are no solutions below a critical antenna current value Above the critical value two solutions exist, one at $n_e = 0$ which is physically irrelevant, and another at some finite electron density This corresponds to a stable inductive mode where the critical current value is the minimum antenna current required to initiate an inductive plasma There is no E-mode or hysteresis in this simplified treatment

3.2 Hysteresis

Hysteresis in the E-to-H transition is believed to be due to non-linearities associated with the power balance equation Hysteresis is obtained when non-linearities are introduced into the dependence of the power absorbed, power dissipated or both, on electron density In this situation P_{dis} and P_{abs} depart from the linear behaviour of figure 3 1 The non-linearities introduced create a second stable operating mode below the maintenance current for an inductive plasma This corresponds to the stable E-mode A range of unstable intermediate operating points exist between the two stable modes as illustrated in figure 3 2 This shows the two stable operating points representing the stable E-mode and the stable H-mode It also shows an unstable intermediate region where either mode is possible In which mode the intermediate region operates depends on the previous history i e if input power is increased from the E-mode to H-mode, the discharge will remain in E-mode through the intermediate region before the transition to H-mode Conversely, if input power is decreased from the H-mode, the discharge will remain in H-mode through the intermediate region before the transition to the E-mode

There are several factors which are believed to be responsible for these non-linearities, and possibly other factors which have not been considered to date Also, the degree to which each contributes to hysteresis is not entirely understood Non-linearities may be divided into two categories, those affecting P_{abs} (circuit non-linearities) and those affecting P_{dis} (plasma non-linearities)

3 2 1 Non-linearities in P_{abs}

The treatment above only considered inductive power coupling, however all 'real' inductive discharges will deposit some power capacitively Capacitive power coupling has a major effect on the power absorbed The effect of capacitive coupling leads

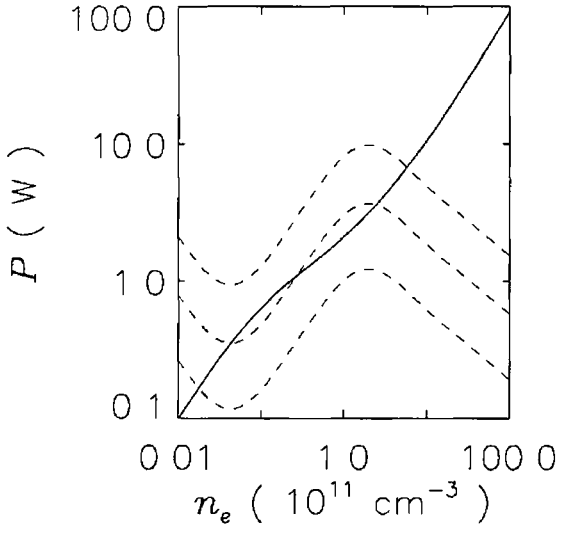

Figure 3 2 *P_{abs} (dashed line), P_{dis} (solid line) as a function of n_e in an inductive discharge including capacitive coupling and other mechanisms affecting hysteresis The three dashed lines now represent P_{abs} for an antenna current in the stable E mode (the lower line), an antenna current in the stable H mode (the upper line), and an antenna current in an unstable intermediate region containing many curve crossings [1]*

to an increase in P_{abs} at low n_e as compared with the purely inductive case, figure (3 2)

Since an inductive plasma discharge may be considered as a one-turn secondary of an air core transformer in the appropriate circuit, capacitive coupling may also be included as a parallel branch of the same circuit Hence, we have two separate branches of a circuit representing the plasma discharge, one for inductively coupled power and one for capacitively coupled power The capacitive coupling leads to an increase in P_{abs} at low electron densities as compared with the purely inductive case

3.2.2 Capacitive Coupling

The introduction of capacitive coupling into the discharge circuit provides an alternative current path for plasma current The partition of current into inductive and capacitive branches introduces a non-linearity into the power absorbed in the discharge due to the fact that the impedance of both inductive and capacitive branches depend on plasma density A non-linearity is also introduced by virtue of the fact that the impedance of the inductive and capacitive branches are dependant upon one another since variation of the capacitive sheath with plasma density will modify the mutual inductance between the primary antenna and secondary plasma Other non-linearities may be introduced involving Child sheath law capacitance and Paschen sheath breakdown [1]

3.2.3 Non-linearities in P_{dis}

In our initial treatment P_{dis} was assumed to be $\propto n_e$, due to the assumption that ε_{T_e} was independent of plasma density This assumption may be valid at low plasma densities but begins to breakdown at higher density as volume collisional processes become involved At higher plasma densities, coulomb collisions between electrons change the eedf from a Druyvesteyn-like distribution (depleted high energy tail), to a more maxwellian distribution with a greater number of higher energy electrons These high energy electrons may deposit more power into the plasma via inelastic processes that require high energy electrons to take place This has the effect of breaking the linear dependence of P_{diss} on n_e The effect of electron-electron collisions with increasing electron density play an important role in the size of the hysteresis At low n_e the eedf has a depleted high energy tail (Druyvesteyn edf) due to the loss of high energy electrons via inelastic processes, and also the fact that only the higher energy electrons may overcome the retarding sheath potential

and escape to the chamber walls As n_e increases, electrons may gain energy via electron-electron collisions thereby replenishing the higher energy electrons in the tail of the eedf The eedf becomes more maxwellian as electron-electron collisions become more prominent This transition from a Druyvesten to Maxwellian eedf creates a non-linearity in the $P_{dis}(n_e)$ and hence contributes to the hysteresis effects observed

Electrons may also ionise the gas through multistep ionisation of atoms in metastable states, which will introduce non-linearities into P_{dis} As electron density increases, more energy is involved in exciting atoms into metastable states, thereby increasing the departure from linear behaviour assumed in our initial treatment A simplified picture of the effect of metastable density within an Ar plasma discharge is to consider the four lowest excited states (two radiative and two metastable levels) as one single state [1] This single state now has two main loss mechanisms, radiative decay to the ground state, and multistep ionisation The loss of atoms in these excited states may be divided into two regimes depending on which loss mechanism is the more dominant At low electron density, electron collisions with metastable atoms are in-frequent, hence the dominant loss mechanism is radiative decay to the ground state At higher electron densities, collisions and hence multi-step ionisation increase thereby making multi-step ionisation the dominant loss mechanism Both regimes lead to extra channels for power dissipation into the plasma discharge increasing the dependence of ε_{T_e} on electron density and hence increasing the non-linearity in $P_{dis}(n_e)$

Non-linearities in power dissipated may arise through multistep ionisation, and the effect of coulomb collisions at high electron density which affect the eedf Both these processes affect plasma production and hence contribute to hysteresis Regardless of the mechanism behind the hysteresis the underlying principle remains the same, that of two stable and one unstable operating points

3.2.4 Transition Dynamics

The dynamics of the E-to-H transition may be broken down into a series of steps We initially look at the electron particle balance equation where electrons are produced in both the capacitive and inductive modes, and lost to the discharge walls

$$\left(\int_V K_{iz} n_g n_e dV\right)_E + \left(\int_V K_{iz} n_g n_e dV\right)_H = \int_S \eta n_e \nu_B dS \qquad (3\ 7)$$

using the notation of [13] We begin with the plasma in a stable E-mode Electrons are produced through ionisations emanating from the capacitive (E) term on the left hand side of (5) As antenna current is increased, the induced electric field becomes sufficient to cause ionisations within the plasma A contribution to electron production is now made from the inductive (H) term on the left hand side of (3 7) At this point the rate of ionisation increases rapidly and is greater than the loss rate to the walls The discharge is now in a state of inequilibrium and is undergoing the transition The rate of ionisation will continue to be greater than the rate of loss until the skin depth sufficiently reduces the induced field (and hence ionisation rate) and equilibrium is regained

3.3 E-to-H experiments

The motivation behind this experiment was to find out the effect of gas mixtures on the E-to-H transition in an Inductively Coupled Plasma Using argon as the background gas, small amounts of molecular gas (oxygen) were added and the effect observed

Initial results were taken manually by increasing the input power through the E-to-H transition and decreasing the input power through the H-to-E transition A Scientific Systems PIM^{TM} was used to record the antenna current at which each transition occurred, over a range of pressures The point at which the transition occurred was determined visually This was repeated using argon with varying percentages of oxygen A graph of transition currents versus gas pressure was obtained for 100% argon and varying percentages of molecular gas The technique was subsequently improved using a power sweep method A LabVIEW^{TM} computer control program was used to vary the input power from minimum to maximum over a fixed period, while simultaneously recording the antenna current over a range of pressures (figure 3 3) The E-to-H and H-to-E transitions were observed from the resulting current trace as a 'glitch' in the antenna current as the load characteristic of the plasma changed from capacitive to inductive (figure 3 4) This method was faster and more accurate than collecting data manually The transition currents versus gas pressure were recorded for 100 % Ar and subsequently for Ar with a mixture of oxygen up to 10 %

3 3 1 E-to-H transition for Argon

Using the above technique we recorded the E-to-H and H-to-E transition currents for a pure argon discharge over a range of neutral gas pressures Shown in figures 3 6 and 3 5 is the E-to-H and H-to-E transition currents as recorded for an ICP

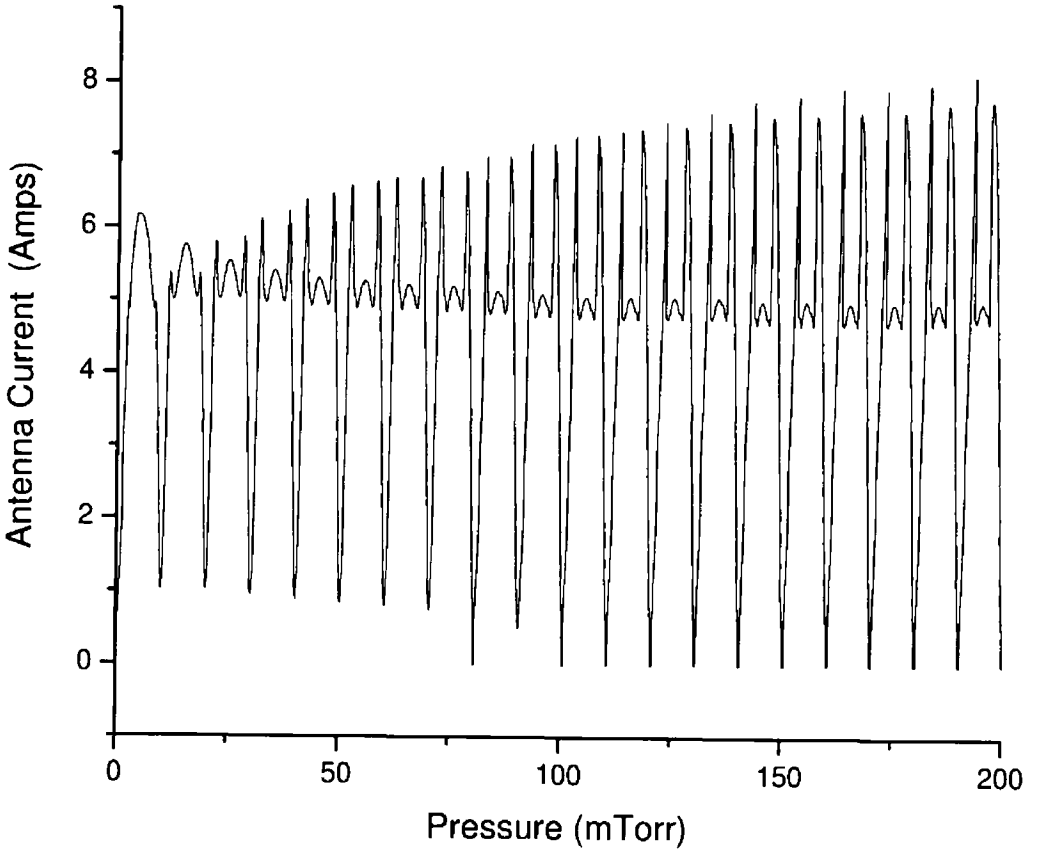

Figure 3 3 *Antenna current as power is swept from minimum to maximum over a pressure range 10 to 200 mTorr*

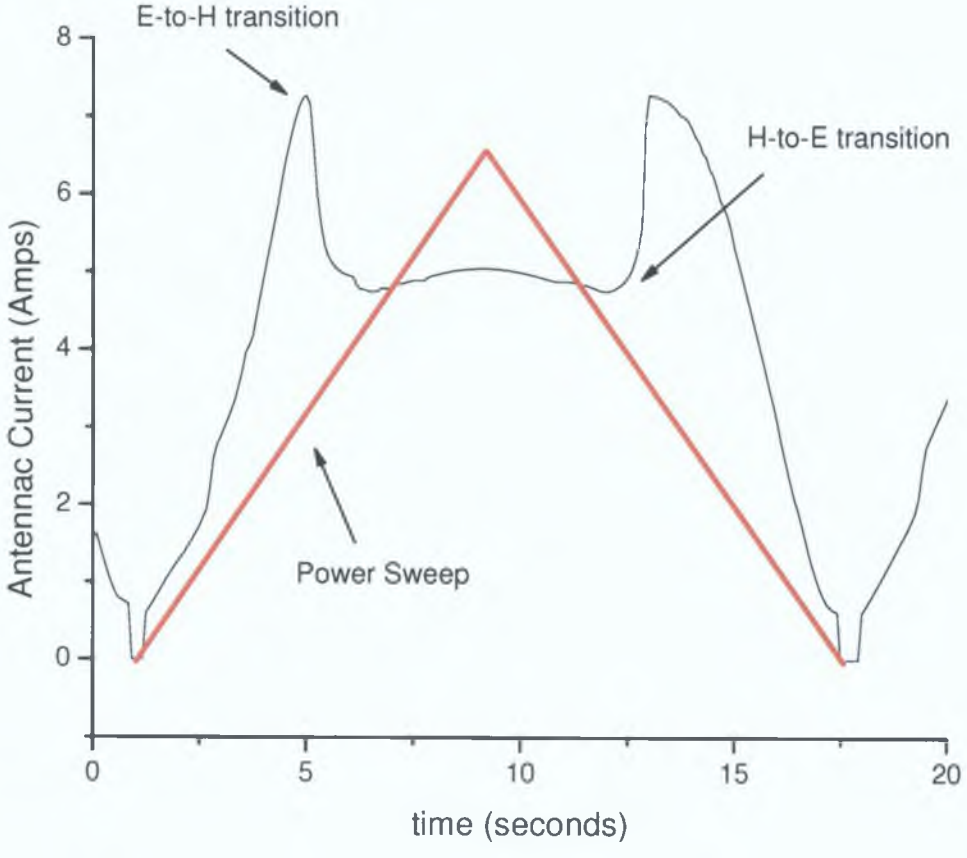

Figure 3.4: *Identification of the E-to-H and H-to-E transition points as a 'glitch' on the antenna current. Also shown is the triangular profile of the power sweep from minimum to maximum power.*

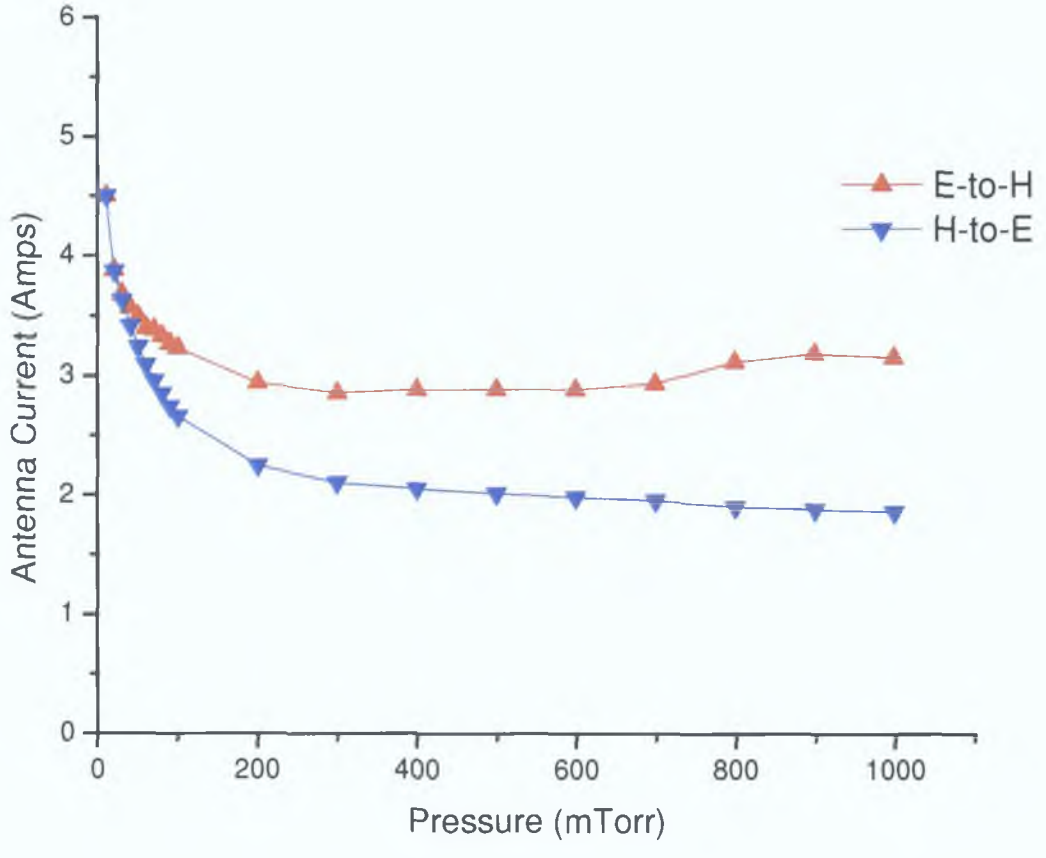

Figure 3.5: *Antenna current at the E-to-H and H-to-E transition points over pressure range 10 to 1000 mTorr*

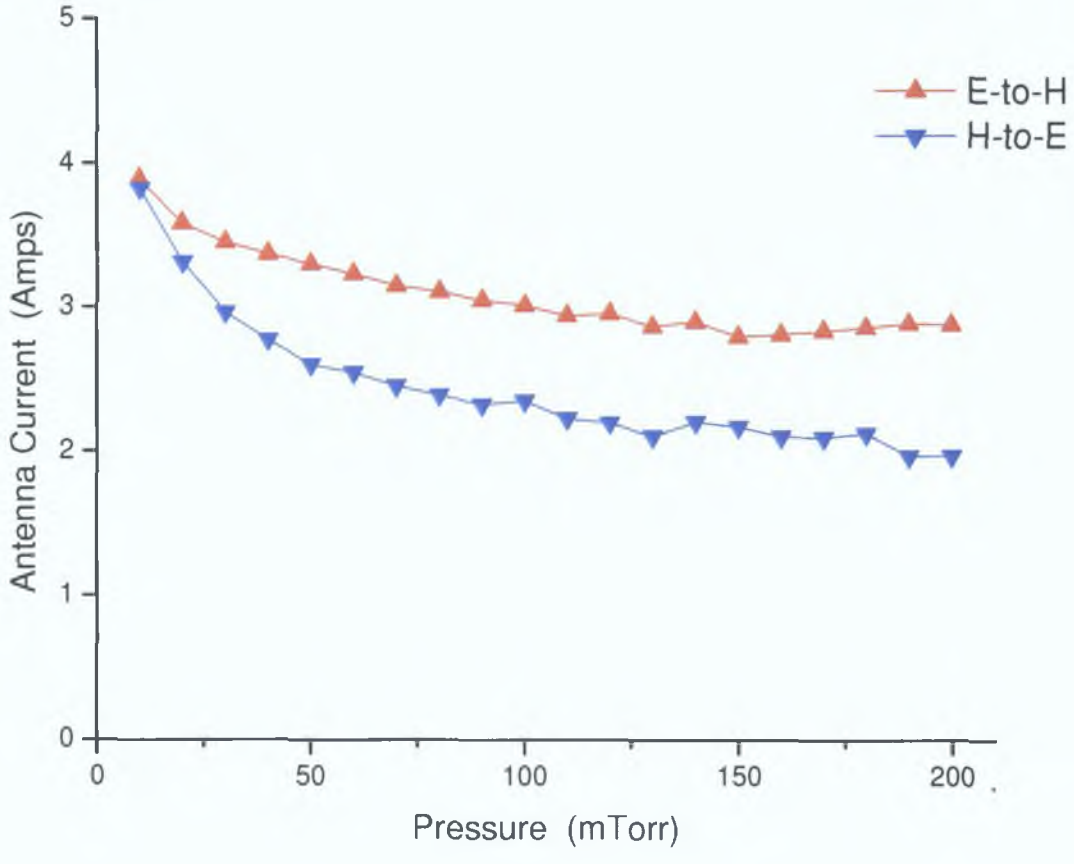

Figure 3.6: *Antenna current at the E-to-H and H-to-E transition points over pressure range 10 to 200 mTorr*

discharge containing 100% argon as a function of pressure

3.3.2 E-to-H transition for Argon/Oxygen mixtures

Also recorded were the E-to-H and H-to-E transition currents for a pure argon discharge over a range of neutral gas pressures with small amounts of molecular oxygen added figures 3 7 and 3 8 Here we can see the effect of small amounts of molecular oxygen on both the ignition current and maintenance current which increases with the addition of oxygen Also we observe the increase m the instability window between the ignition and maintenance currents

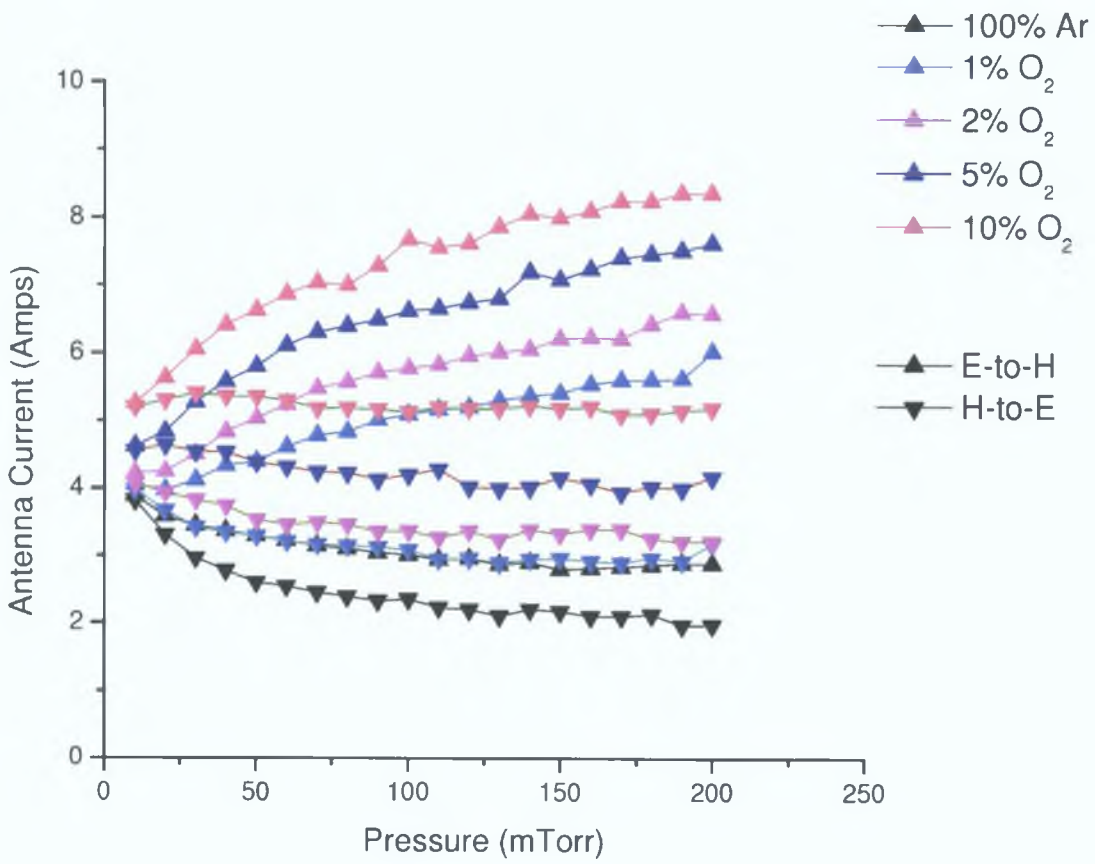

Figure 3.7: *E-to-H transition for 100 % Argon and Argon/Oxygen mixtures over a pressure range of 10 - 200 mTorr*

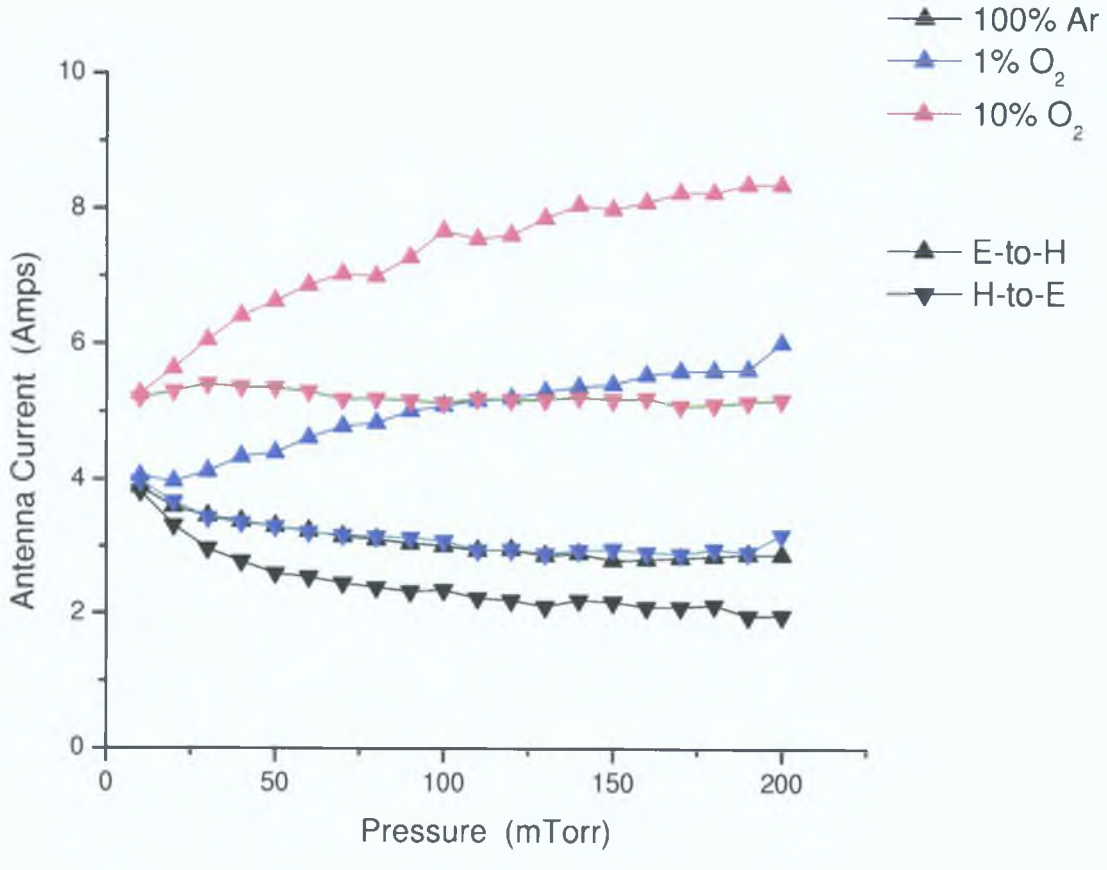

Figure 3.8: *E-to-H transition for 100 % Argon and Oxygen mixtures over a pressure range of 10 - 200 mTorr*

3.4 Argon Global Model

In the following chapter we detail the global models used in this work The global model used in this work is based on a standard global model as used by Lieberman *et al* [17, 18] In this model a volume averaged (global) model in a cylindrical discharge of length l and radius R is considered In this simple model the main assumptions are Ions are considered to be stationary (ion temperature$T_i = 0$), Only collisional ionisation is considered i e no excitation is incorporated in to the model

The rate equations to be solved are the electron particle balance 3 8 and the electron energy balance equation 3 9

$$\frac{dn_e}{dt} = k_{iz} n_e n_g - \Gamma_e A_{eff}/V \tag{3 8}$$

$$\frac{3}{2}\frac{d}{dt}(n_e T_e) = P_{abs} - P_{loss} \tag{3 9}$$

which may be re-arranged using the differentiation product rule to give

$$\frac{dT_e}{dt} = \frac{2}{3}\frac{P_{abs} - P_{loss}}{n_e} - \frac{T_e}{n_e}\frac{dn_e}{dt} \tag{3 10}$$

Equations 3 8 and 3 10 may be integrated to obtain $n_e(t)$ and $T_e(t)$ In the following section we will outline the appropriate details used in 3 8 and 3 10

3 4 1 Model equations

In order to describe the equations used in the global model we will describe them in terms of levels Level 1 will describe the unknowns in the rate equations, level 2 will introduce the unknowns in level 1 and so on We will first describe the model equations in the electron particle balance (3 8), and then the electron energy balance (3 10)

3.4 2 Electron Particle Balance

In this section we outline the equations required in the electron particle balance equation 3 8

Level 1 equations

The unknowns in the electron particle balance equations are $n_e, n_g, k_{iz}\Gamma_e, A_{eff}, V$ which are the electron density in m^{-3}, gas density in m^{-3}, ionisation rate constant in $m^3 s^{-1}$, electron flux in $m^{-2}s^{-1}$, effective area of the plasma in m^2, and the discharge volume in m^3, respectively

The ionisation rate constant, k_{iz} is given in the Arrhenius form [13]

$$k_{iz} = k_{iz0} e^{-\varepsilon_{iz}/T_e} \tag{3 11}$$

where ε_{iz} is the ionisation energy for argon (15 759 eV) and the pre-exponential factor, K_{iz0}, is found experimentally to be $\simeq 5 \times 10^{-14} m^3 s^{-1}$ [13]

The electron flux, Γ_e is given by

$$\Gamma_e = \frac{1}{4} n_e \overline{v_e} e^{-\Phi/T_e} \tag{3 12}$$

where $\overline{v_e}$ and ϕ are the average electron velocity and plasma sheath potential respectively These will be detailed in the next section

The gas density, n_g is obtained from the isothermal equation of state for an equilibrium Maxwellian distribution (ideal gas law)

$$n_g = \frac{P}{k_B T_g} \tag{3 13}$$

where P, k_b and T_g are the gas pressure, boltzmann constant and gas temperature respectively

The effective plasma area, A_{eff} is found from low pressure plasma diffusion theory and is given by [13]

$$A_{eff} = 2\pi R^2 h_l + 2\pi R l h_R \tag{3 14}$$

where R is the radius, and l is the length of the discharge chamber h_l and h_R are the edge-to-center density ratios as found from low pressure diffusion theory and outlined in the next section

Finally the volume, V, is simply given by $V = \pi R^2 l$

Level 2 equations

The average electron velocity is obtained by integrating the Maxwellian velocity distribution over all velocities to obtain

$$\overline{v} = \left(\frac{8eT_e}{\pi m_e}\right)^{\frac{1}{2}} \tag{3 15}$$

The plasma sheath potential is given by [13]

$$\Phi = -T_e Ln\left(\frac{M_i}{2\pi M_e}\right)^{\frac{1}{2}} \tag{3 16}$$

The edge-to-center density ratios are found from low-pressure diffusion theory and are given by the equations

$$h_l = 86\left(3 + \frac{1}{2\lambda_i}\right)^{-\frac{1}{2}} \tag{3 17}$$

$$h_R = 8\left(4 + \frac{R}{\lambda_i}\right)^{-\frac{1}{2}} \tag{3 18}$$

where λ_i is the ion mean free path given by $\lambda_i = 1/n_g\sigma_i$ where ion-neutral cross section, $\sigma_i \simeq 1 \times 10^{-18} m^2$ [13]

3.4.3 Electron Energy Balance

In this section we outline the required equations in the electron energy balance equation 3 9

Level 1 equations

The unknowns in the electron energy balance equation are the power absorbed by the plasma (P_{abs}) and the power lost to the plasma wall (P_{loss}) The power lost is given by

$$P_{loss} = n_e n_g k_{iz} \epsilon_{iz} + \Gamma_e(\Phi + 2T_e)\frac{A_{eff}}{V} \tag{3 19}$$

The first term on the right hand side describes the volume ionisation and the second term on the right hand side describes the energy loss for positive ions that are accelerated across the sheath potential Φ, and accounts for the kinetic energy of the ions carried to the walls All terms have been previously described above

The power absorbed consists of inductively coupled power and capacitively coupled power

$$P_{abs} = P_{ind} + P_{cap} \tag{3 20}$$

which may be given as

$$P_{abs} = I_{rf}^2 R_{abs}\frac{n_e n_0}{n_e^2 + n_0^2}\frac{1}{V} + I_{rf}^2 R_{abs}\frac{n_e}{n_e + n_c}\frac{1}{V} \tag{3 21}$$

where the first term on the right hand side corresponds to the inductive power and the second term corresponds to the capacitive power n_e, I_{rf} and V are the plasma density, antenna current and plasma volume respectively n_c, n_o and R_{abs} are arbitrary values chosen to best describe power absorption [19] Justification for these values is described in more detail in Chapter 6

3 4 4 Global Model Results

The global model described above illustrates ICP discharge behaviour including capacitive coupling The temporal evolution of electron density is shown in figure 3 9 Here we see the temporal evolution of electron density to a steady state for two different antenna current values One antenna current is in the capacitive mode and the other is in the inductive mode We note that the steady state value of the H-mode is $\sim$ 2-3 orders of magnitude greater than that of the E-mode, as expected The evolution of the electron temperature is also illustrated for two antenna current values One in the capacitive mode and the other in the inductive mode In figure 3 10 the temporal evolution of the electron temperature differs in the two regimes at early time but settles to approximately the same value in the steady state This is as expected from the global model assumption that the electron temperature is a function of gas pressure and discharge dimensions and is independent of electron density

The E-to-H transition is illustrated more clearly in figure 3 11 Here the steady state electron density is shown as a function of antenna current Each point in the graph is the result of the steady state global model for that particular antenna current In this figure the E-to-H transition is clearly indicated as an electron density 'jump' of $\sim 2 - 3$ orders of magnitude over a small change in antenna current

We also illustrate the effect of gas pressure on the E-to-H transition as taken from the global model in figure 3 13 Here we see the reduction in antenna maintenance current from a 50 mTorr to a 1000 mTorr ICP The behaviour is more clearly illustrated in figure 3 14 where the E-to-H transition current is plotted as a function of pressure Also illustrated is the H-to-E, calculated as the maintenance current from equation 5 18 Comparing the experimental (figure 3 12) and model (figure 3 14) results we see qualitative agreement between model and experiment for the 100% argon case An extension of the model to include Ar/O_2 mixtures may achieve

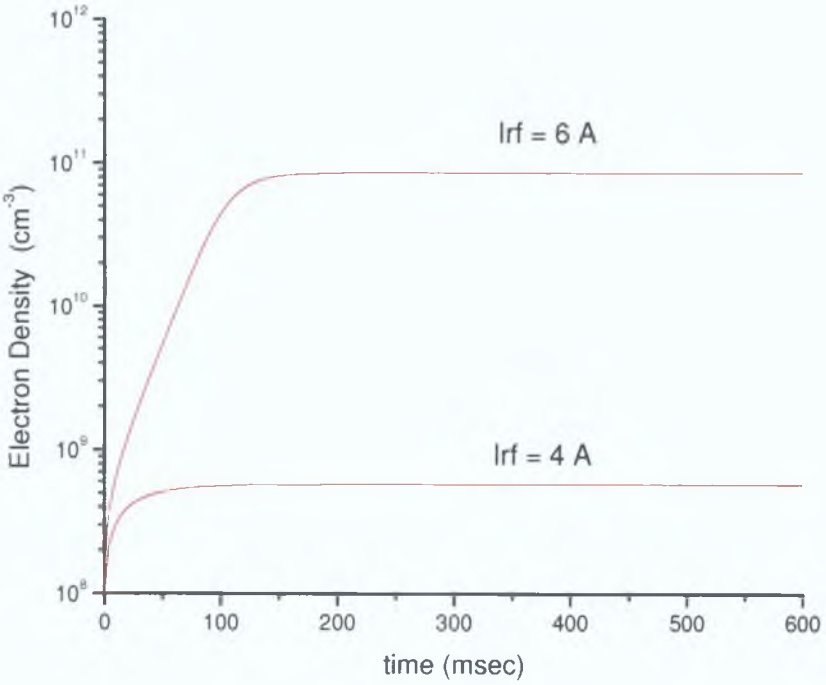

Figure 3.9: *Global Model results of the time evolution of electron density. Shown are the results for two antenna currents:* $I_{rf} = 4A$ *in the capacitive mode and* $I_{rf} = 6A$ *in the inductive mode.*

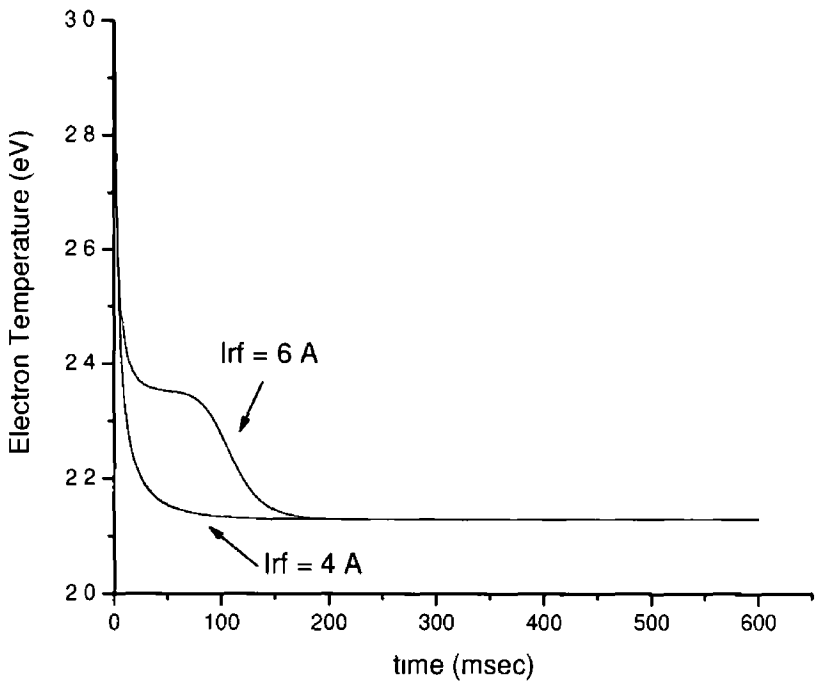

Figure 3 10 *Global Model results of the time evolution of electron temperature Shown are the results for two antenna currents $I_{rf} = 4A$ in the capacitive mode and $I_{rf} = 6A$ in the inductive mode*

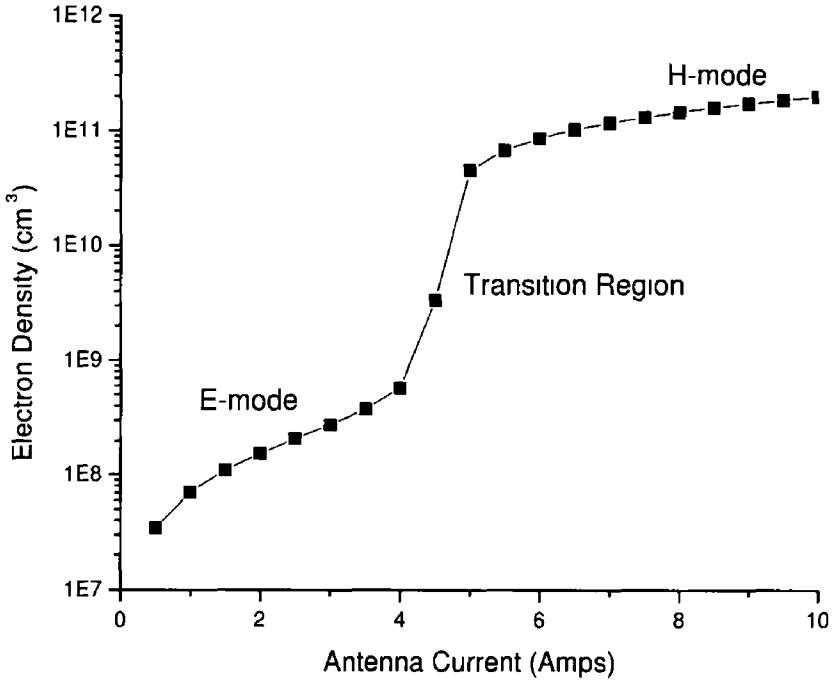

Figure 3 11 *Global Model results of the steady state electron density as a function of antenna current Shown are the low density E-mode, the high density H-mode and the transition region*

similar agreement with the Ar/O_2 experimental results

3.5 ICP electromagnetic model

Characterisation of an ICP plasma requires an understanding of the electric and magnetic fields within the discharge region To this end we present an analysis of the electric and magnetic fields within the discharge chamber under vacuum and in the presence of a plasma The analysis follows closely the technique of El-Fayoumi et al [20] applied to the geometry of the BARIS system see figure 3 15

We initially consider only the inductive mode and ignore capacitive coupling The solenoid acts as a helical antenna radiating electromagnetic waves at the standard industrial frequency of 13 56 MHz ($\lambda \approx 22$ m) Our analysis begins by considering the appropriate Maxwell's equations appertaining to Faraday's law (3 22) and Ampere's law (3 23)

$$\nabla \times \mathcal{E} = -\frac{\partial \mathcal{B}}{\partial t} \tag{3 22}$$

$$\nabla \times \mathcal{B} = \mu_0 \sigma \mathcal{E} + \epsilon_0 \frac{\partial \mathcal{E}}{\partial t} \tag{3 23}$$

Combining 3 22 and 3 23 under appropriate assumptions allows us to obtain an analytical expression for the E and B fields in both vacuum and in the presence of a plasma

E and B fields in Vacuum

It is customary to consider E and B fields in vacuum as being coupled leading to the propagation of an electromagnetic wave However the standard industrial operating frequency of 13 56 MHz ($\sim$ 22 m) places the wavelength of the propagating wave outside the discharge chamber In this case we may ignore the displacement current

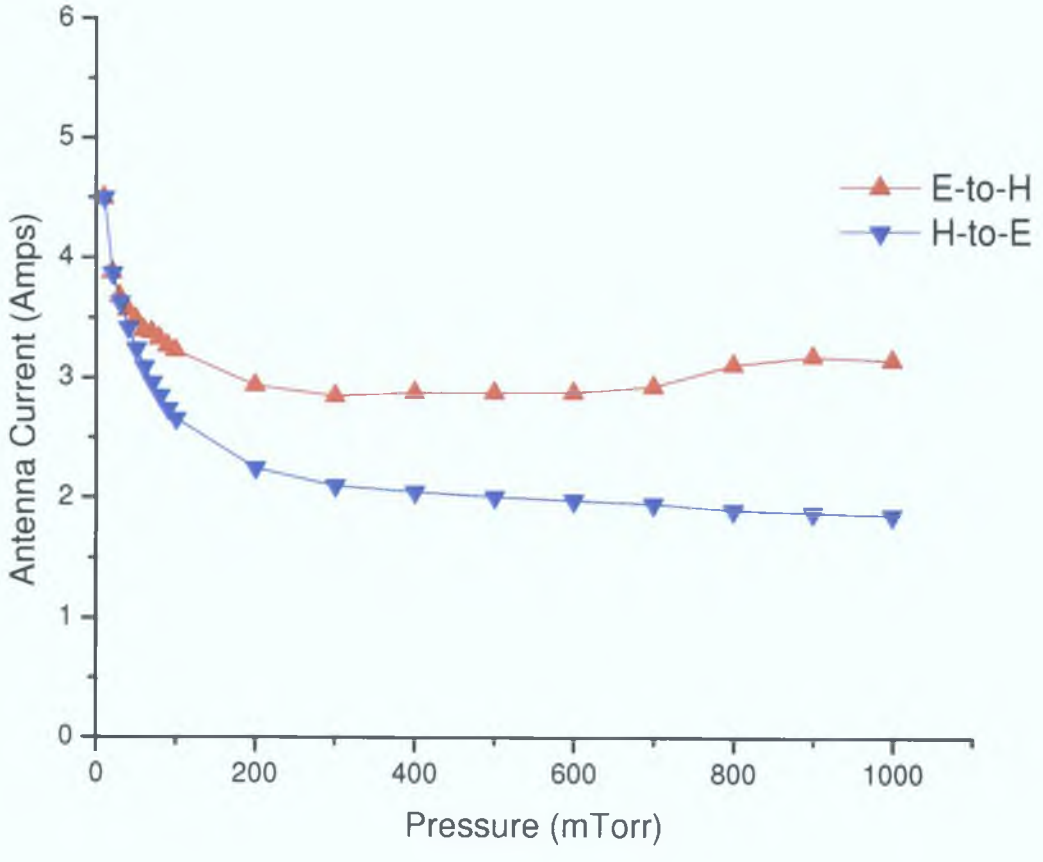

Figure 3.12: *Antenna current as power is swept from minimum to maximum over a pressure range 10 to 1000 mTorr*

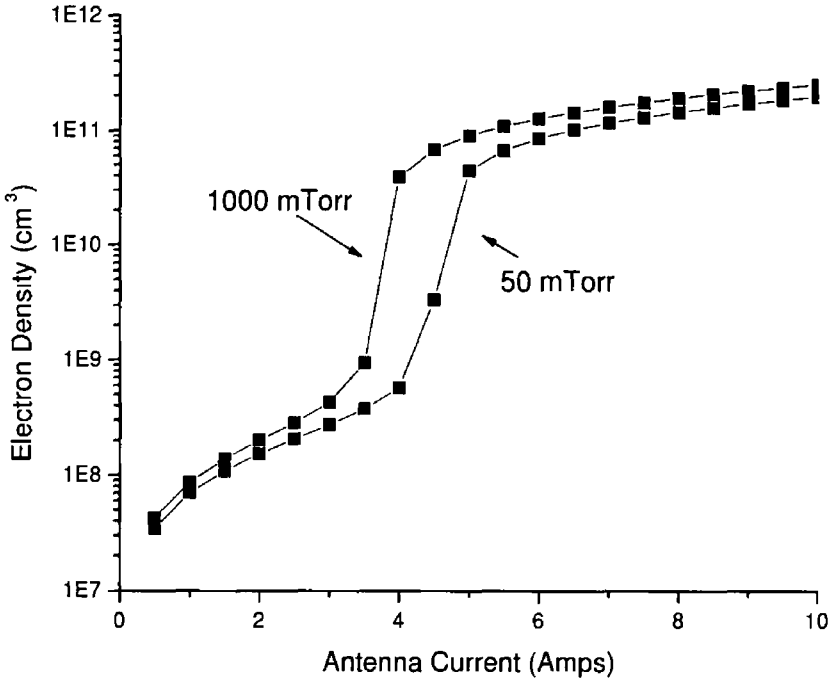

Figure 3 13 *Global Model results of the steady state electron density as a function of antenna current for pressures 50mTorr and 1000mTorr This illustrates a reduction in antenna current for the E-to-H transition with increasing pressure consistent with experimental observations*

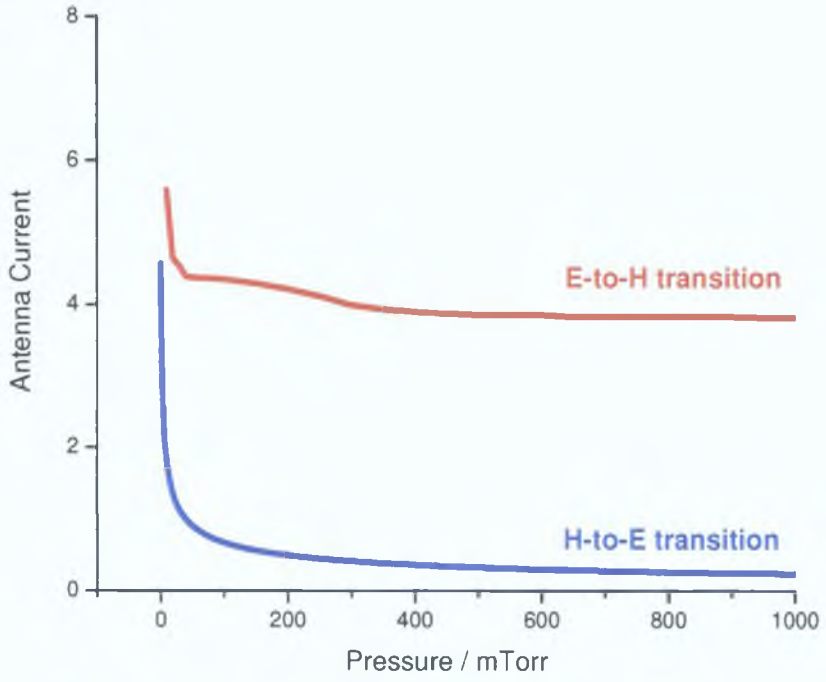

Figure 3.14: *Shown are the calculated maintenance current (H-to-E transition) and the global model calculation of the E-to-H transition current as a function of pressure.)*

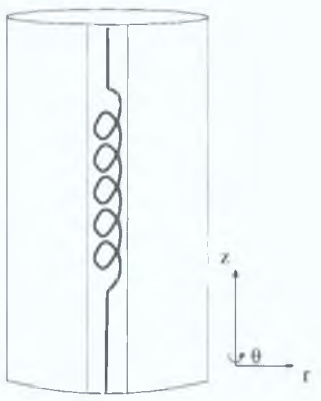

Figure 3.15: *Simplified representation of BARIS system*

($\epsilon_0 \frac{\partial \mathbf{E}}{\partial t}$) in equation 3 23 Standard procedure is to take the curl of one equation and substitute into the other to obtain an expression for the E or B field as a function of position assuming a time dependence of the form $e^{\imath\omega t}$ Assuming the E and B fields both have a time dependence of the form $e^{\imath\omega t}$ in cylindrical co-ordinates, we may write

$$\mathcal{E}(r,\theta,z,t) = \mathbf{E}(r,\theta,z)e^{\imath\omega t} \tag{3 24}$$

$$\mathcal{B}(r,\theta,z,t) = \mathbf{B}(r,\theta,z)e^{\imath\omega t} \tag{3 25}$$

Combining with 3 22 and taking the curl of both sides leads to

$$\nabla \times \mathbf{E} = -\imath\omega\mathbf{B} \tag{3 26}$$

and

$$\nabla \times \nabla \times \mathbf{E} = -\imath\omega\sigma\mathbf{E} \tag{3 27}$$

Using cylindrical symmetry we may assume that the E and B fields have the following components, $E \equiv \{0, E_\theta, 0\}$ and $B \equiv \{B_r, 0, B_z\}$ In cylindrical coordinates, the curl of a vector field E, is given by

$$\nabla \times E = \left(\frac{1}{r}\frac{\partial E_z}{\partial \theta} - \frac{\partial E_\theta}{\partial z}\right)\hat{r} + \left(\frac{\partial E_r}{\partial z} - \frac{\partial E_z}{\partial r}\right)\hat{\theta} + \frac{1}{r}\left(\frac{\partial}{\partial r}(rE_\theta) - \frac{\partial E_r}{\partial \theta}\right)\hat{z} \tag{3 28}$$

and

$$\begin{aligned}\nabla \times \nabla \times E \;=\; & \left[\frac{1}{r}\frac{\partial}{\partial \theta}\left(\frac{1}{r}\frac{\partial}{\partial r}(rE_\theta) - \frac{\partial E_r}{\partial \theta}\right) - \frac{\partial}{\partial z}\left(\frac{\partial E_r}{\partial z} - \frac{\partial E_z}{\partial r}\right)\right]\hat{r} + \\ & \left[\frac{\partial}{\partial z}\left(\frac{1}{r}\frac{\partial E_Z}{\partial \theta} - \frac{\partial E_\theta}{\partial z}\right) - \frac{\partial}{\partial r}\left(\frac{1}{r}\frac{\partial}{\partial r}(rE_\theta) - \frac{\partial E_r}{\partial \theta}\right)\right]\hat{\theta} + \\ & \frac{1}{r}\left[\frac{\partial}{\partial r}(r)\left(\frac{\partial E_r}{\partial z} - \frac{\partial E_z}{\partial r}\right) - \frac{\partial}{\partial \theta}\left(\frac{1}{r}\frac{\partial E_z}{\partial \theta} - \frac{\partial E_\theta}{\partial z}\right)\right]\hat{z}\end{aligned} \tag{3 29}$$

Considering only the azimuthal ($\hat{\theta}$) component and assuming azimuthal uniformity, equation 3 27 becomes

$$-\frac{\partial^2 E_\theta}{\partial z^2} - \frac{1}{r}\frac{\partial}{\partial r}(rE_\theta) + \frac{E_\theta}{r^2} = -i\omega\mu_0\sigma E_\theta \tag{3 30}$$

Similarly separating the $\hat{r}$ and $\hat{z}$ components in equation 3 26 leads to

$$-i\omega B_r = -\frac{\partial E_\theta}{\partial z} \tag{3 31}$$

and

$$-i\omega B_z = \frac{1}{r}\frac{\partial(rE_\theta)}{\partial r} \tag{3 32}$$

We may now obtain analytical solutions for the E and B fields An expression for E_θ may be obtained from 3 30 using the separating of variables technique

3.6 Summary

In the preceding chapter an introduction to the present understanding of the E-to-H transition was given outlining the relevant physics The results of several experiments were presented detailing ICP behaviour in relation to pure argon discharges and argon/oxygen mixtures A global model was introduced and the results compared to experimental results illustrating qualitative agreement in the pure argon case An extension of the global model to include argon/oxygen mixtures was not carried out but would be possible and may be carried out in future work

CHAPTER 4

Plasmoid Characterisation

Plasmoids are a commonly observed plasma phenomenon in industrial discharges They may be loosely defined as a localized volume of higher plasma density and light intensity exhibiting some type of ordered structure Observed examples include structures such as rings, spokes, disks or spheres which may be either stationary or rotating Although many examples of plasmoids have been observed, the physical mechanism responsible is not well understood and little literature exists The term "Plasmoid" was provisionally coined by R W Wood [8] as far back as 1930 where he observed luminous balls, spindles and pear shaped bodies in an inductively coupled vacuum tube discharge In our discharge, plasmoids are observed within the E-to-H instability window and their behaviour is affected by changes in this window In this chapter we outline the characterisation as carried out by Crowley [2] and further characterisation in particular relating to rotation of plasmoids under various conditions

4.1 Present understanding of plasmoids

Little theoretical work has been carried out on plasmoid formation Most of the knowledge to date stems from experimental observation Due to the variant nature of the phenomena it is impractical to comment on experimental systems other than our own Extensive experimental work has been carried out on the cylindrical BARIS experiment by B Crowley *et al* [2] The plasmoids are described as bright regions or 'lobes' arranged symmetrically within the discharge, and may rotate in either direction Depending on experimental conditions they may number anything from two lobes to ten lobes Rotation rate depends on power and pressure and has been measured as high as 60 Hz Although rotation is possible in either direction, clockwise rotation appears to be the preferred direction It was found that direction of rotation was independent of the direction of coil windings in the antenna The number of observable lobes (mode number) depends on power, pressure and gas mixture However this is a non-trivial dependence and exhibits bi-stability and complex hysteresis cycles Langmuir probe measurements were taken in an argon discharge at 200 mTorr and 50 W input power with three lobes present They revealed that the ratio of electron densities between dark and bright regions was 53 with a plasmoid density of $1\,5 \times 10^{11}$ Measurements of electron temperature across the lobe revealed an almost constant average temperature, however the high energy tail was enhanced inside the plasmoid region

An I/V probe inserted between the match unit and antenna was used to record the antenna current during the mode 'jumps' between successive mode numbers The antenna current at which the $I_{n\to n\pm1}$ is shown in figure 4 1

The plasmoid threshold current also show a pressure dependence (figure 4 2) At pressures below 500 mTorr, modes 2 and 3 are dominant, with modes 3 and 4 becoming more dominant at higher pressures Plasmoid behaviour also shows a strong frequency dependence with the onset of plasmoid behaviour at 11 MHz

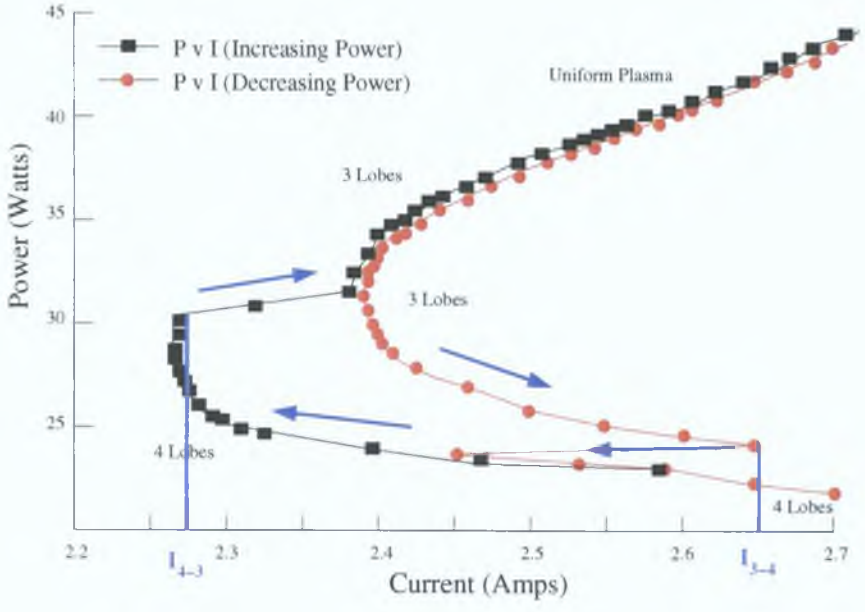

Figure 4.1: *Absorbed power as a function of antenna current. The black curve is taken with increasing power and the red curve is taken with decreasing power. [2]*

occurring at 60 mTorr with the corresponding behaviour at 13.56 MHz at 200 mTorr.

The effect of absorbed discharge power versus electron density (figure 4.3) also showed that the relationship between absorbed power and electron density is different in the low power (instability) regime as opposed to the high power (stable) regime.

Gas composition also plays a role in plasmoid formation. It has been observed that the addition of a small amount ($1 \sim 2$ %) of oxygen radically changes the nature of the discharge (figure 4.4). With the addition of oxygen, the plasmoids form at lower pressures,over a wider range of power and more modes were observed.

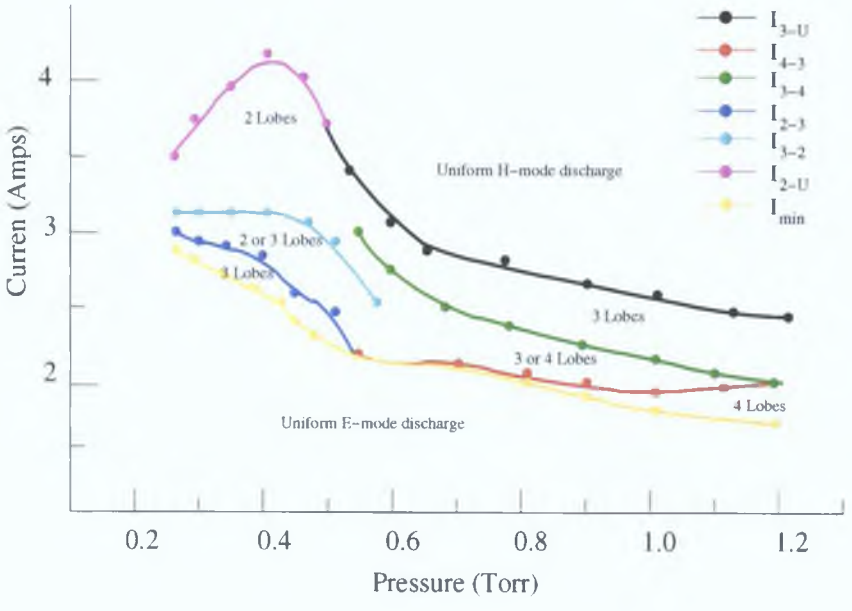

Figure 4.2: *Transition currents for various mode numbers as a function of pressure. Also indicated is the mode number observed in each region [2].*

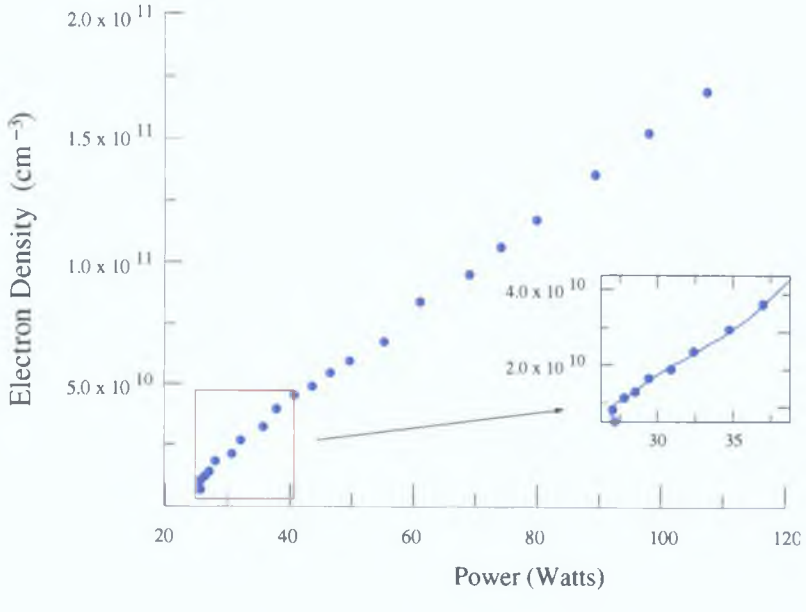

Figure 4.3: *Electron density as a function of absorbed power [2].*

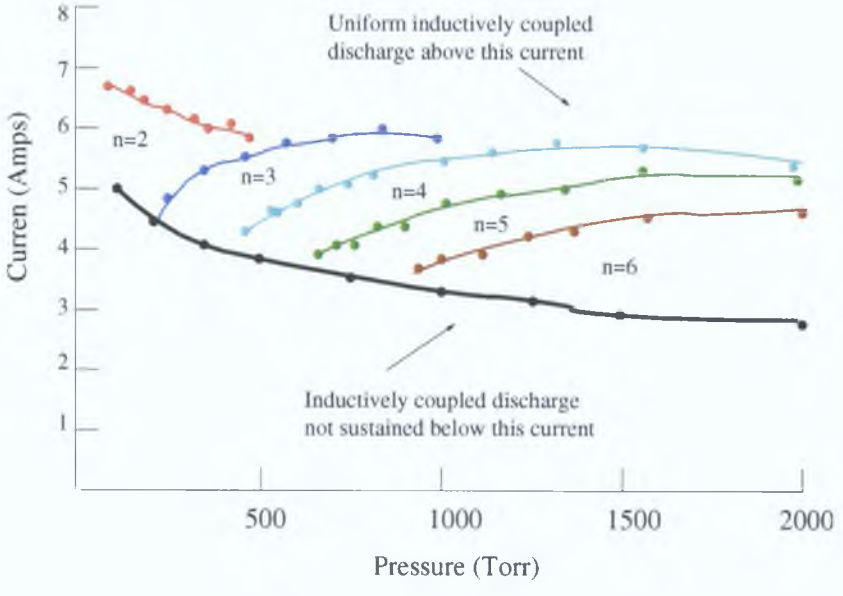

Figure 4.4: *Transition currents for various mode numbers as a function of pressure. Also indicated is the mode number observed in each region of 98% Ar - 2% O_2 discharge [2]*

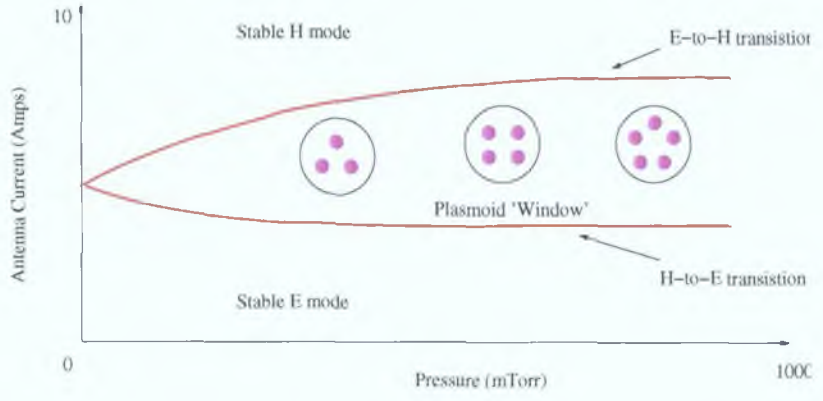

Figure 4.5: *Illustration showing the E-to-H transition region as a function of pressure and antenna current. The plasmoid form within this 'window'*

4.2 Characterisation of Plasmoid Rotation

The following section outlines the characterisation of plasmoid rotation in an ICP. The rotation of plasmoid lobes was measured using a Photo-Multiplier Tube (PMT) which detected a collimated beam of light emitted in the radial direction of the discharge chamber (figure 4.6). Plasmoid rotation is in the azimuthal direction allowing the rotation frequency to be calculated as the frequency as measured by the PMT divided by the number of lobes.

4.3 Plasmoid Rotation as a function of Pressure

In this experiment the plasmoid rotation frequency was measured as a function of gas pressure. The system parameters were optimised to obtain a reasonable number of plasmoid lobes over the desired pressure range. This required adjusting the input power to position the system in an appropriate position in the plasmoid window (figure 4.5) upon which the input power was held constant for the duration of the experiment. The system was setup and plasmoid rotation was measured using the

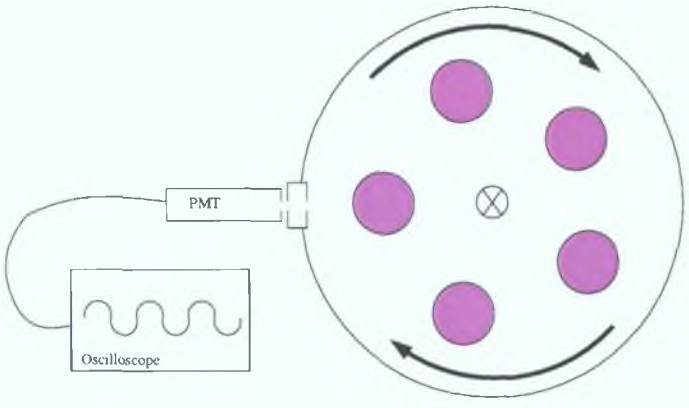

Figure 4.6: *The rotation frequency of the plasmoids was captured using a Photo Multiplier Tube (PMT) linked to an oscilloscope. The rotation frequency in the azimuthal direction was calculated as the frequency measured by the PMT divided by the number of lobes*

photomultiplier tube for a range of pressures between 10 and 1000 mTorr. The procedure was carried out in an argon discharge with mixtures of molecular oxygen. For each gas mixture the input power had to be adjusted to obtain plasmoids in the power and pressure range that exhibited rotation. The results of the experiment are shown in figure 4.7. Here we can see that as pressure increases the rotation rate slows for a particular number of lobes. As pressure is increased the number of lobes increases by one causing the rotation rate to decrease dramatically demonstrating the transitional nature of plasmoids. As pressure is increased further the rotation rate begins to increase as before until the next mode jump where upon it decreases dramatically again. This behaviour is most striking in the mixture of 10% oxygen where plasmoids are easily obtained and available over a wider parameter range. The behaviour is still evident though, in the mixtures with lower concentrations of oxygen.

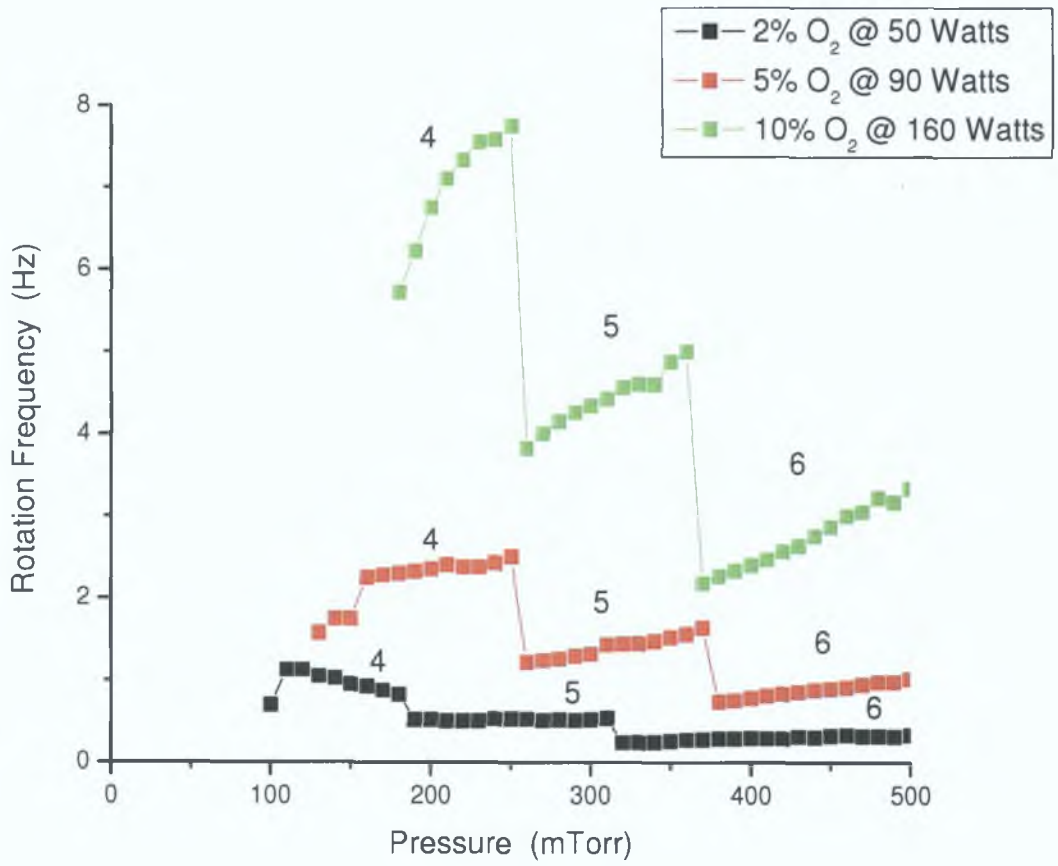

Figure 4.7: *Plasmoid rotation as a function of gas pressure*

4.4 Plasmoid Rotation as a function of Gas Mixture

In this experiment the plasmoid rotation is measured as a function of gas mixture added to an argon plasma During the experiment the gas pressure is held constant using the PID control loop which controls the Mass Flow Controllers (MFCs) The input power is adjusted to maintain fixed input power and is arbitrarily chosen in order to obtain the maximum number of plasmoids available at a particular pressure The rotation frequency was measured using the PMT system as before for a plasmas containing 100% argon The rotation rate was recorded as a function of the ratio of oxygen / argon mixtures while maintaining constant input power and pressure The oxygen mixture was varied from 1 t0 10% as increasing the oxygen content caused the plasma to be extinguished for the given input power The effect of gas mixture on flow rate is shown in figure 4 8 for varying powers and pressures

4.5 Phase Resolved Spectroscopy of an Inductive Plasma

Figure 4 9 shows the experimental setup for modulation of light on the BARIS system An RF amplifier is driven using at 13 56 MHz using a signal generator A second signal generator, phase locked with the primary, is used to trigger the Intensified Charge Coupled Device (ICCD) system The second signal generator is needed due to a quirk in the ICCD software which does not allow multiple periods of the incoming frequency to the pulse delay generator to be scanned This is overcome by using a signal of one quarter the frequency and phase locked to the primary RF signal generator This allows four RF (13 56 MHz) periods to be scanned

The optical fibre is placed end-on parallel to the antenna on the BARIS chamber

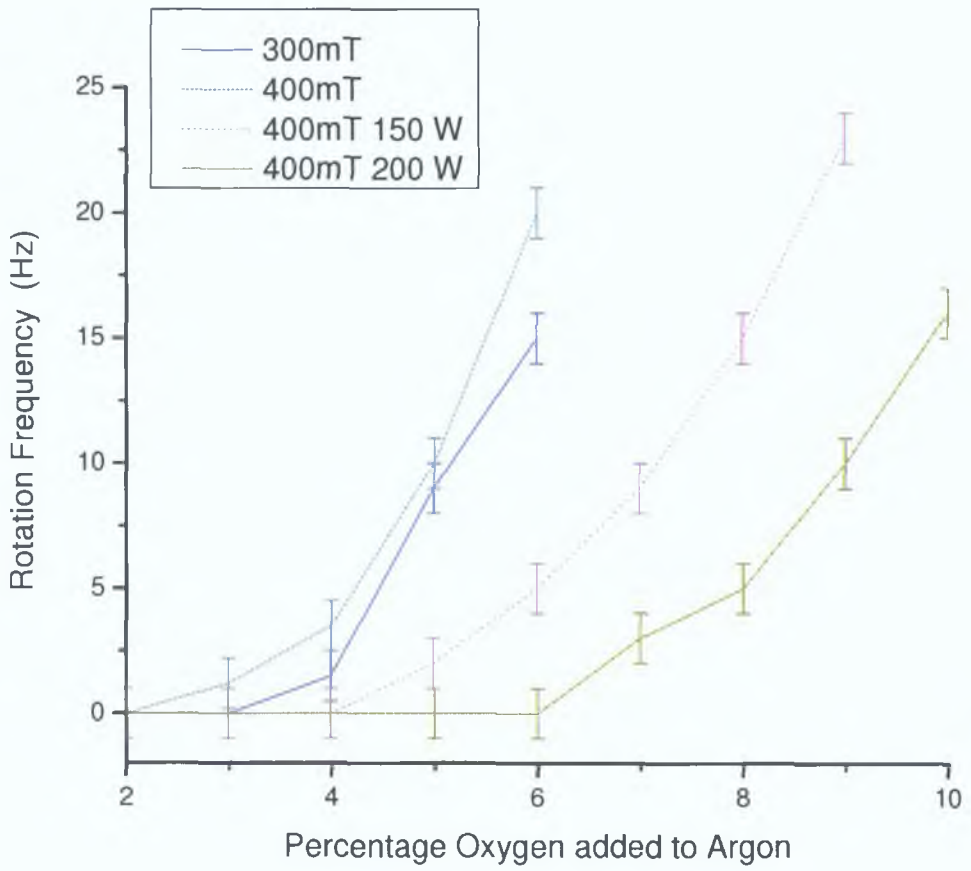

Figure 4.8: *Plasmoid Rotation as a function of Pressure*

with no focussing optics The fibre was tested at three positions along the radial axis of the cylindrical system at basically inner, middle and outer positions

During each scan, the system was setup to scan across 4×13 56 MHz periods (295 ns) at 5 ns increments At each phase, the integration time was 2000 ms and 15 averages were taken The entire 295 ns 'run' took approximately 35 minutes

A pure Neon plasma was tested using the 585 2 nm line (14 5 ns lifetime) Modulation was clearly observed using Ne (figure 4 10) However we have, as yet, been unable to obtain plasmoids in a Neon plasma

A pure argon plasma was also tested using the lines 750 37 (22 47 ns lifetime) and 811 53 (30 21 ns lifetime) However no definite modulation was observed Both these lines are Neutral Ar transition, there are faster transitions (15 ns) in singly ionised Ar however we could not observe these lines m our discharge

4.6 Summary

In the preceding chapter, experimental characterisation of plasmoid behaviour was detailed The characterisation outlined the work of Crowley[2] illustrating a plasmoid map showing the parameter space in which plasmoids are observed Further characterisation relating to plasmoid rotation was also carried out by investigating rotation as a function of gas pressure and gas mixture A final experiment was briefly introduced illustrating phase resolved optical emission spectroscopy in a Neon discharge

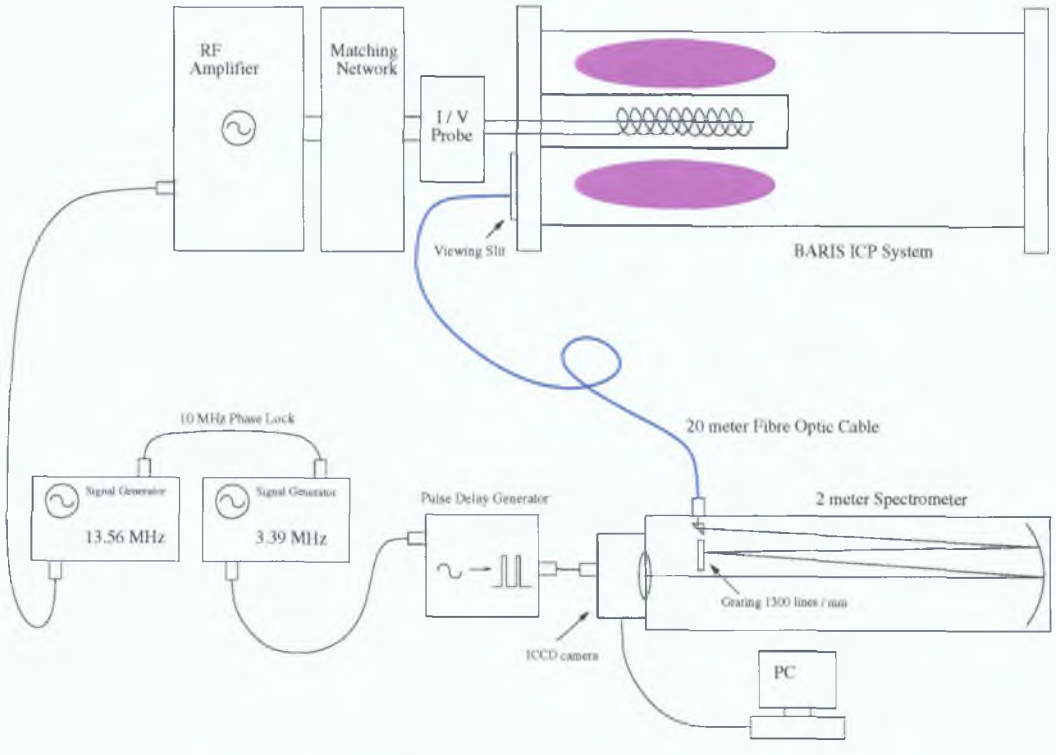

Figure 4.9: *Phase Resolved Spectroscopy experimental setup.*

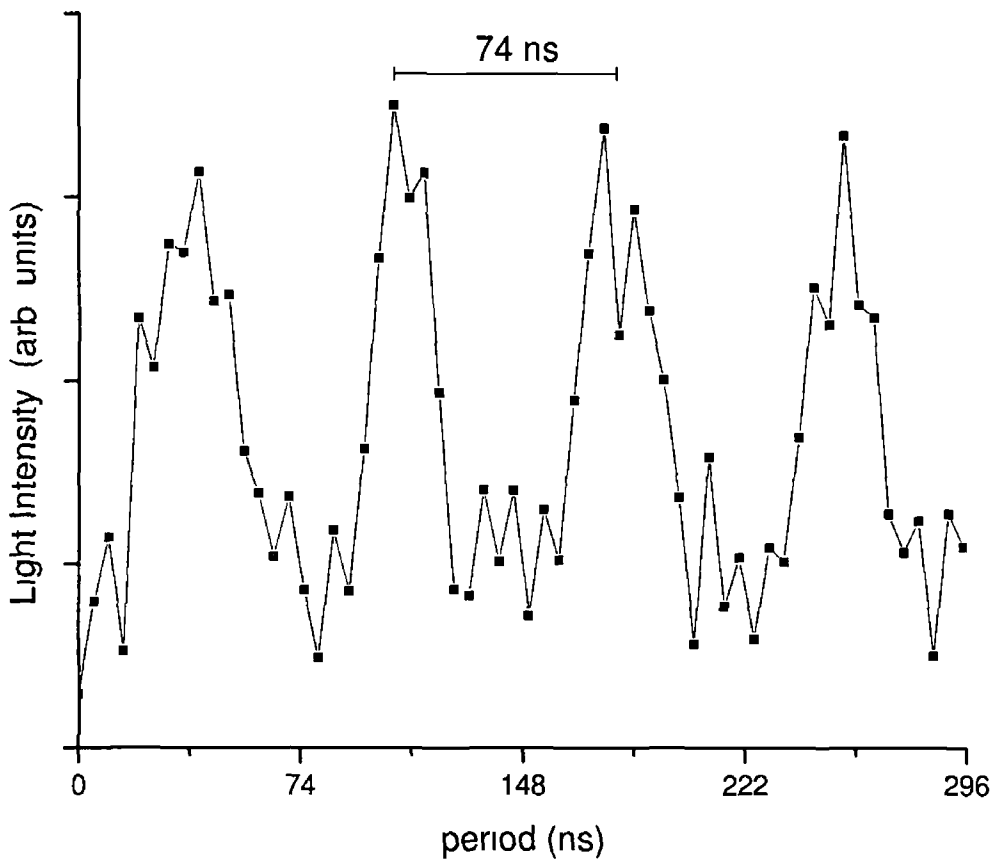

Figure 4 10 *Phase Resolved Modulation of light in an Neon ICP*

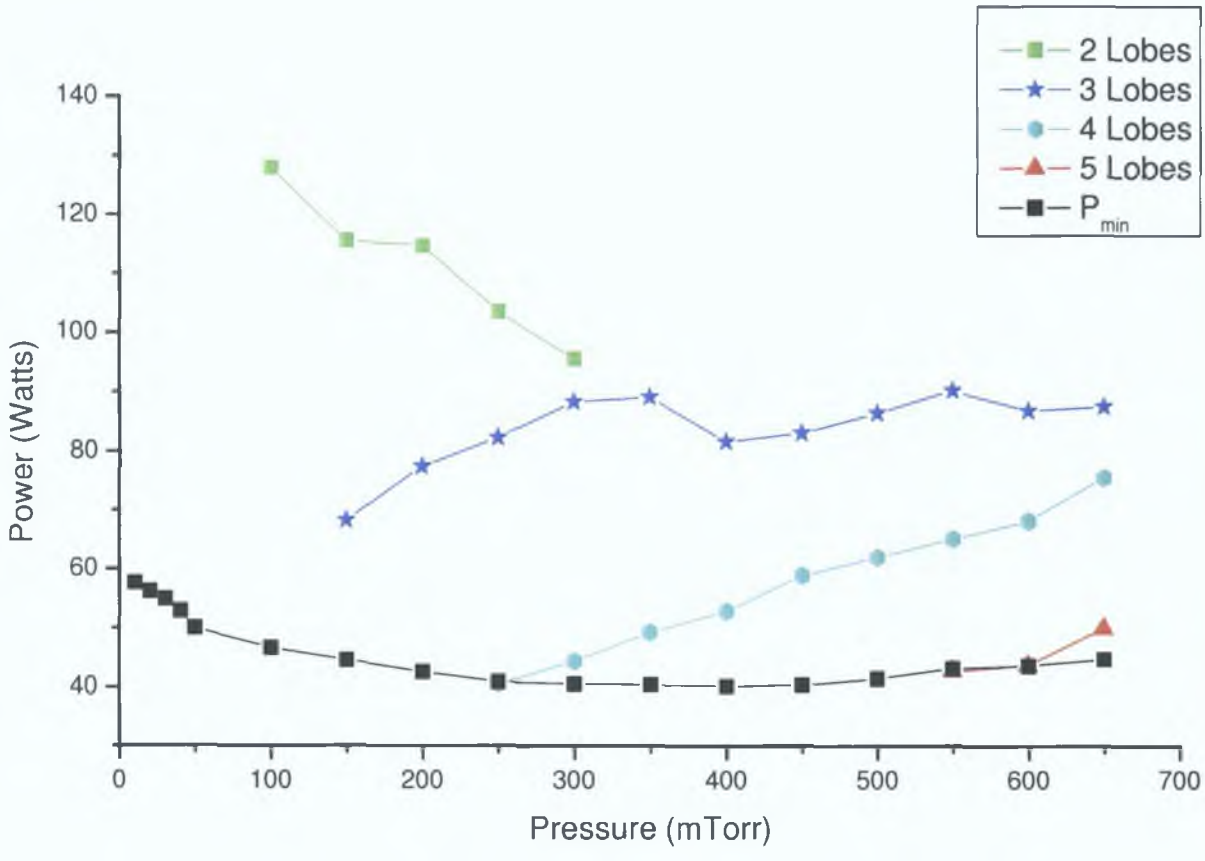

Figure 4.11: *Plasmoid map in an Ar ICP*

CHAPTER 5

Plasmoid Model

In this chapter, we introduce a theoretical model to explain the experimental characterisation of plasmoid behaviour as detailed in the previous chapter. The model presented below accounts for the stationary behaviour of plasmoids as a function of neutral gas pressure and antenna current.

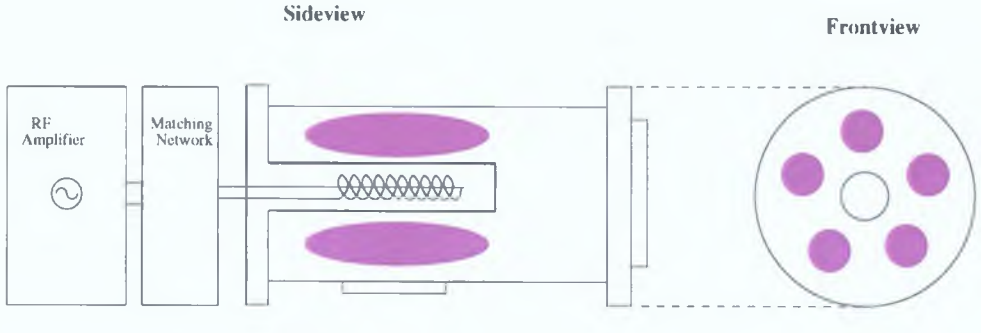

Figure 5.1: *Sideview and Frontview of the BARIS chamber illustrating plasmoid lobes surrounding the antenna*

We propose that the plasmoids observed in ICP systems are wave like or transmission line effects due to the division of power between capacitive and inductive power deposition We consider the transmission line to follow the induced electric field path around the azimuthal direction, with plasma inductance due to inductive coupling in the azimuthal direction, and plasma capacitance due to capacitive coupling in the radial direction Since the plasma current path is closed, it may be represented as an infinite transmission line with a series inductance and parallel capacitance

5.1 ICP Transmission Line Model

The transmission line model is designed to model the BAsic Radiofrequency Inductive Source (BARIS) BARIS consists of a helical antenna centered co-axially inside a cylindrical stainless steel discharge chamber (figure 5 1) The antenna is isolated from the discharge inside a quartz dielectric tube using a re-entrant configuration [16]

The separated and total current paths are shown in figure 5 2 The capacitive current path is shown in figure 5 2(a) as a capacitive sheath and a plasma resistance going from the high voltage antenna to the grounded discharge chamber The inductive current path is shown in figure 5 2(b) as a plasma resistance due to the geometrical and electron inertia inductance travelling in the azimuthal (θ) direction These are combined to elicit the spatial behaviour of the plasma as 'lumped' circuit elements in figure 5 2(c) Finally the total current paths are 'opened' out to show a standard transmission line representation in figure 5 2(d)

An infinite transmission line of this configuration may be modelled as a propagating wave travelling in an infinitely long medium which has variable phase velocity In this situation the medium is the transmission line and the phase velocity at any

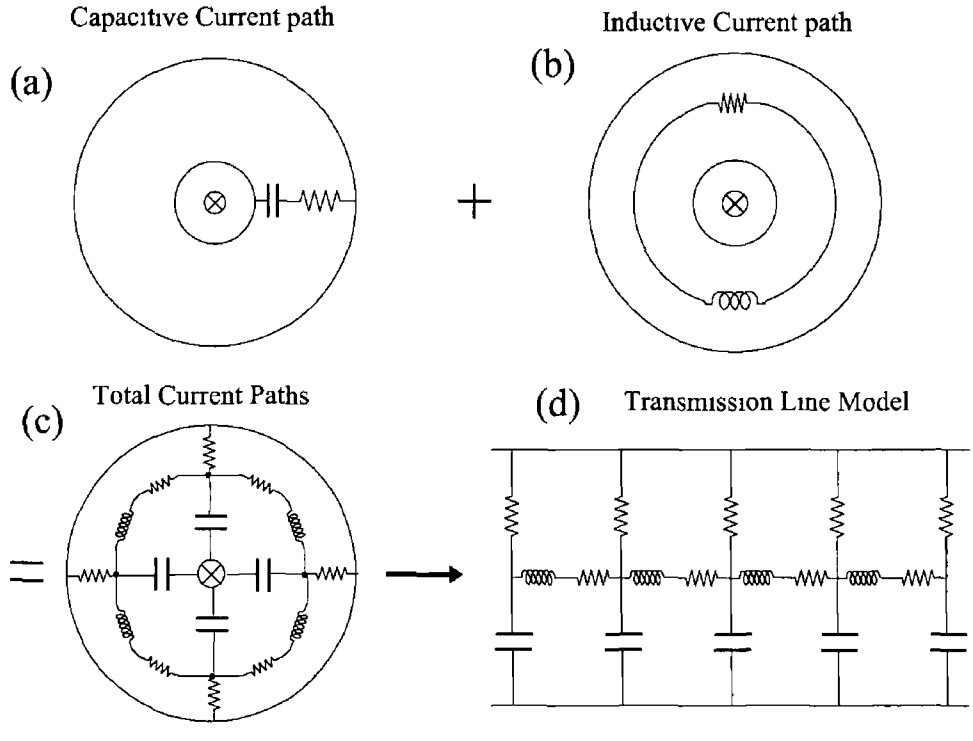

Figure 5 2 *(a) The capacitive current path through the capacitive sheath and through the ohmic resistor (b) The inductive current path with an ohmic resistor and an inductor representing the geometrical inductance and electron inertia inductance (c) The combination of capacitive and inductive current paths (d) The opened out representation showing the transmission line model*

given point is determined by the plasma capacitance and plasma inductance at that point If the phase velocity has a co-sinusoidal variation in space, then the system may be modelled by Mathieu's equation [21]

5.2 Mathieu's Equation

Mathieu's equation is a special case of a linear second order homogenous differential equation which has numerous applications in physics and engineering [22] Its original application was as a mathematical description of vibrations on an elliptical membrane [23] and has since been used in a variety of physical situations such as an inverted pendulum, stability of a floating body, and vibrations in a medium with modulated density It is in the application of vibrations in a medium with modulated density that we wish to use Mathieu's equation, but first we will outline the pertinent details of the equation

Mathieu's equation is usually written in the form

$$\frac{\partial^2 y}{\partial z^2} + (a - 2q\cos 2z)y = 0 \tag{5 1}$$

where 'a' and 'q' are assumed to be real constants in physical applications Particular values of 'a' and 'q' lead to characteristic solutions of equation 5 1 which are periodic in z with period π or 2π Non characteristic values of 'a' and 'q' lead to two types of solution which are either unstable (i e infinite as $z \to \pm\infty$), or non-periodic According to Floquet's theorem [24], solutions to Mathieu's equation exists in the form

$$y(x) = exp(i\gamma x)f(z) \tag{5 2}$$

where γ is a function of 'a' and 'q' and f(z) is a periodic function of period π or 2π If γ is an integer then the solution is periodic, if γ is a real non-integer then the solution is not periodic but stable, if γ is imaginary then the solution is unstable In relation to our application of Mathieu's equation to wave propagation in a medium of modulated density, the periodic, non-periodic and unstable solutions correspond to standing waves, waves in the pass band and waves in the stop band respectively Since γ is a function of 'a' and 'q' we may plot a map of 'a' and 'q' space and see this visually (figure 5 3) Stationary solutions ce_n and se_n correspond to even and odd

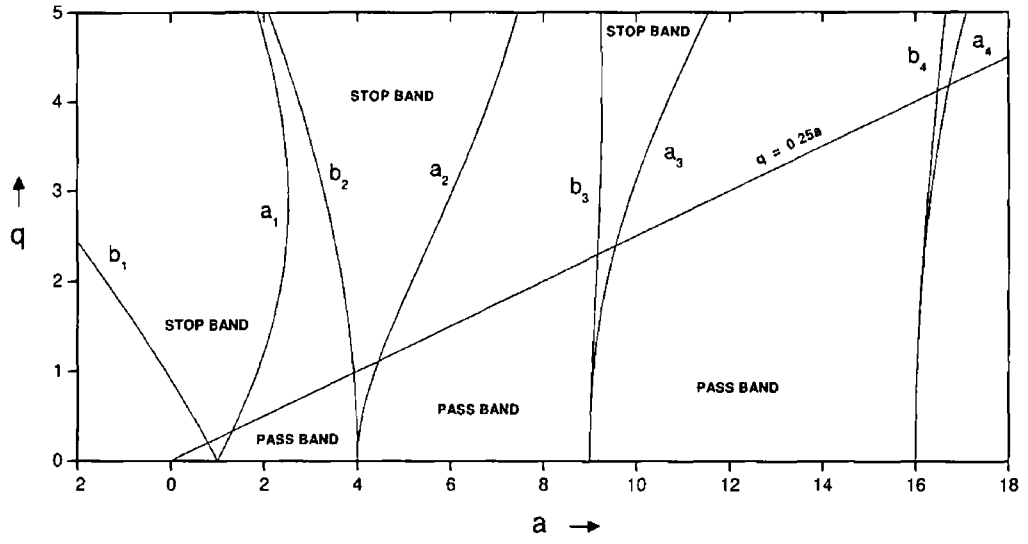

Figure 5 3 *Mathieu map of a vs q Solid lines show the standing wave solutions to Mathieu's equation*

solutions respectively, to Mathieu's equation for a given set of characteristic values 'a' and 'q' The ce and se solutions are known as cosine elliptical and sine elliptical analogous to cosine and sine solutions of a simple harmonic oscillator equation to which 5 1 reduces for q = 0 The regions between the solutions order ce_n and se_n correspond to values of 'a' and 'q' which give a complex γ leading to an unstable solution and hence called the stop bands The regions between ce_n and se_{n+1} correspond to regions of 'a' and 'q' which give non integer real value of γ leading to non-periodic but stable solution, and hence called the pass bands The solutions ce_n and se_n are standing wave solutions of order n

5.3 Mathieu's Equation applied to an ICP

For this work, we use the procedure by Cross [21] to describe one-dimensional wave propagation in a medium where the phase velocity varies continuously and periodically and show that this can be modelled using Mathieu's equation The 1D wave equation is

$$\frac{\partial^2 y}{\partial x^2} = \frac{1}{v_p}\frac{\partial^2 y}{\partial t^2} \tag{5 3}$$

Letting $\partial^2 y/\partial t^2 = \omega y$ where ω is the sinusoidal driving frequency, and introducing a co-sinusoidally varying phase velocity over period d, then 5 3 becomes

$$\frac{\partial^2 y}{\partial x^2} + \frac{\omega^2}{v_p^2} y = \frac{\partial^2 y}{\partial x^2} + \omega^2 \left(A - 2B\cos\frac{2\pi x}{d}\right) y = 0 \tag{5 4}$$

The medium is defined by the two constant coefficients A and B Letting $z = \pi x/d$, $a = \omega^2 d^2 A/\pi^2$ and $q = \omega^2 d^2 B/\pi^2$ then equation 5 4 reduces to equation 5 1

As outlined above certain values of 'a' and 'q' correspond to standing wave solutions to equation 5 4 Using the method of Cross [21] we see that a standing wave solution exists for $a = 1, 4, 9, 16$ etc (figure 5 3) We wish to use the results above to show that standing waves may form in an ICP discharge leading to the formation of plasmoids The discussion above shows that

$$a = \frac{\omega^2 d^2 A}{\pi^2} \tag{5 5}$$

with $A = \frac{1}{v_{phase}^2}$ where v_{phase} is the phase velocity of the propagation wave through the medium The phase velocity for a transmission line is given by $v_{phase} = \frac{1}{\sqrt{L_p C_p}}$ where L_p and C_p and the plasma inductance and plasma capacitance respectively The distance over which the periodic distortion occurs is d For a uniform discharge this distance is simply the circumference around a circle defined by the plasma We wish to model the behaviour of the rf power as a function of gas pressure for a value corresponding to a standing wave solution of equation 5 4 Since $a = \omega^2 d^2/\pi^2 v_{phase}^2$,

the two variables are d and v_{phase} We shall treat their dependance on power and pressure as follows

5.4 Phase velocity as a function of pressure

The phase velocity, v_{phase}, of a transmission line is given by

$$v_{phase} = \frac{1}{\sqrt{L_p C_p}} \tag{5 6}$$

Where the plasma capacitance C_p is assumed constant and the plasma inductance L_p, is given by

$$L_p = \frac{\mu_o \pi \delta(\delta + 2R)}{l} \tag{5 7}$$

with skin depth δ, given by

$$\delta = \left(\frac{2M_e \nu_{eff}}{\omega \mu_o e^2 N_e}\right)^{\frac{1}{2}} \tag{5 8}$$

The effective electron-neutral collision frequency (ν_{eff}) as a function of pressure is given by [25]

$$\nu_{eff} = 2\,58 \times 10^{-6}\left(\frac{eT_e}{k_b}\right) + 2\,25 \times 10^{-17}\left(\frac{eT_e}{k_b}\right)\frac{P}{k_b T_g} 1 \times 10^{-6} \tag{5 9}$$

where P is pressure in mTorr The electron density, N_e, is found from

$$N_e = \frac{P_{diss}}{e u_B \epsilon_T A_{eff}} \tag{5 10}$$

Both ν_{eff} and N_e are functions of the electron temperature, T_e which in turn is a function of pressure T_e as a function of pressure is calculated using the standard relation [13]

$$\frac{K_{iz}(T_e)}{u_B(T_e)} = \frac{1}{n_g d_{eff}} \tag{5 11}$$

where K_{iz} is given by [26] and the Bohm velocity $u_B = (\frac{eT_e}{M_{Ar}})$ T_e as a function of pressure is shown in figure 5 4 We can now calculate the phase velocity as function of pressure

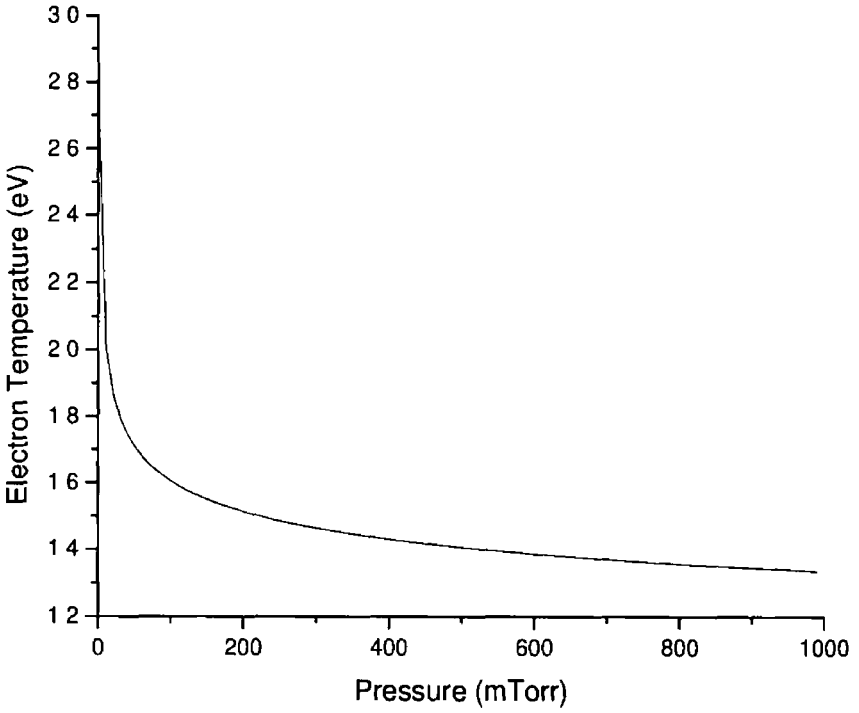

Figure 5 4 *Electron temperature, Te, as a function of pressure*

5.5 Transmission line length as a function of pressure

We now calculate the distance, d The distance d is taken as being the circumference of circle of radius defined as half the skin depth penetration into the plasma

$$d = \frac{2\pi(R + \frac{\delta}{2})}{n} \tag{5 12}$$

where n defines the mode number of the discharge The skin depth has the same pressure dependence as described above therefore we now have d as a function of pressure We use a numerical solver to solve

$$a = \frac{\omega^2 d^2}{\pi^2 v_p^2} \tag{5 13}$$

and obtain power as a function of pressure (figure 5 5) for constant a Repeating the process for standing wave values of a = 4, 9, 16, 25 as taken from fig 5 3

5.6 Minimum maintenance power

The power absorbed by an inductively coupled plasma at low electron density given by the expression [13]

$$P_{abs} = \frac{\frac{1}{2} I_{rf}^2 N_e v_{eff} \pi e^2 \mu_0 N^2 R^4}{8 M_e l} \tag{5 14}$$

where I_{rf} is the antenna current and all other symbols have their usual meaning For a stable plasma to exist, the power absorbed by the plasma (P_{abs}) must balance the power dissipated in the plasma (P_{diss})

$$P_{abs} = P_{diss} \tag{5 15}$$

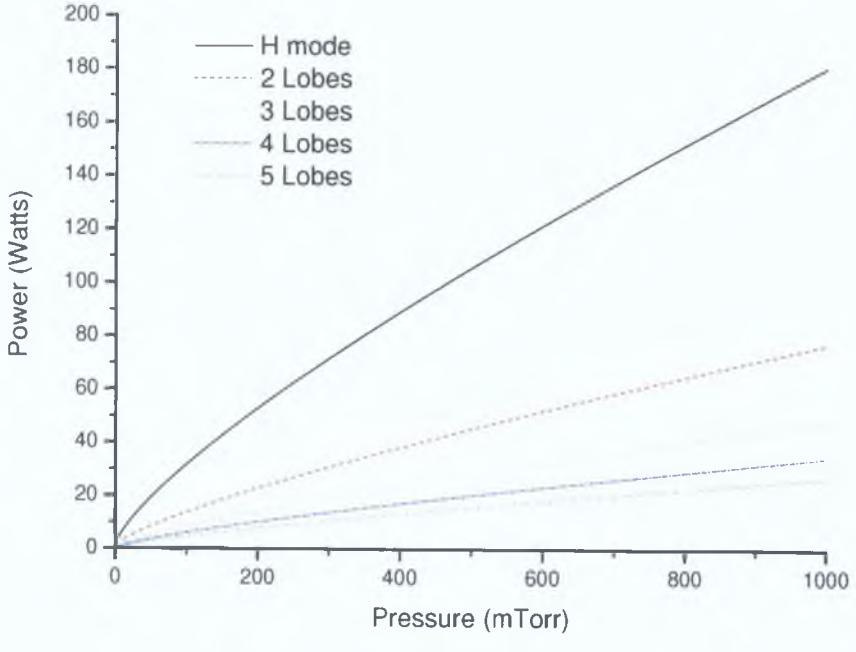

Figure 5.5: *Power Vs Pressure for constant a = 1,4,9,16,25*

where the power dissipated by the plasma electrons is given by [13]

$$P_{diss} = en_e u_B A_{eff} \epsilon_{Ie} \tag{5 16}$$

where u_B is the Bohm velocity, A_{eff} is the effective surface area of the plasma and ϵ_{Ie} is the energy lost per electron-ion pair created in the discharge

At low electron density the minimum rf current required to maintain an inductive discharge is given by the relation

$$\frac{\partial P_{abs}}{\partial N_e} = \frac{\partial P_{diss}}{\partial N_e} \tag{5 17}$$

Solving for I_{rf} gives an expression for the minimum maintenance current I_{rfmin}

$$I_{rfmin} = \left(\frac{u_B \varepsilon_{Ie}}{\nu_{eff}}\right)^{\frac{1}{2}} \left(\frac{16 A_{eff} M_e l}{\pi e^2 \mu_0^2 N^2 R^4}\right)^{\frac{1}{2}} \tag{5 18}$$

The second term in on the right hand side of equation 5 18 is constant The first term contains three variables the Bohm velocity (u_B) which is function of electron temperature T_e , the effective electron-neutral collision frequency (ν_{eff}) which is a function of T_e and pressure P, and the total energy lost per electron-ion pair (ε_{Ie}) which is a function of T_e Using the same procedure as in section 5 4 we obtain the electron temperature as a function of pressure and use this to obtain the minimum maintenance current as a function of pressure (figure 5 6) Although we assume I_{min} is independent of electron density, we still require a finite N_e to determine the power absorbed into the plasma at the minimum maintenance power Assuming a stable inductive discharge is only obtained when the skin depth confines the electromagnetic wave to a region within the discharge chamber, we determine minimum electron density to be that at a skin depth which is a significant fraction of the chamber radius i e where $\delta \simeq \frac{R_{chamber}}{n}$ where $R_{chamber}$ is the radius of the discharge chamber and $n \simeq 1 \rightarrow 3$ We may now plot the minimum maintenance power as a function of pressure figure 5 7

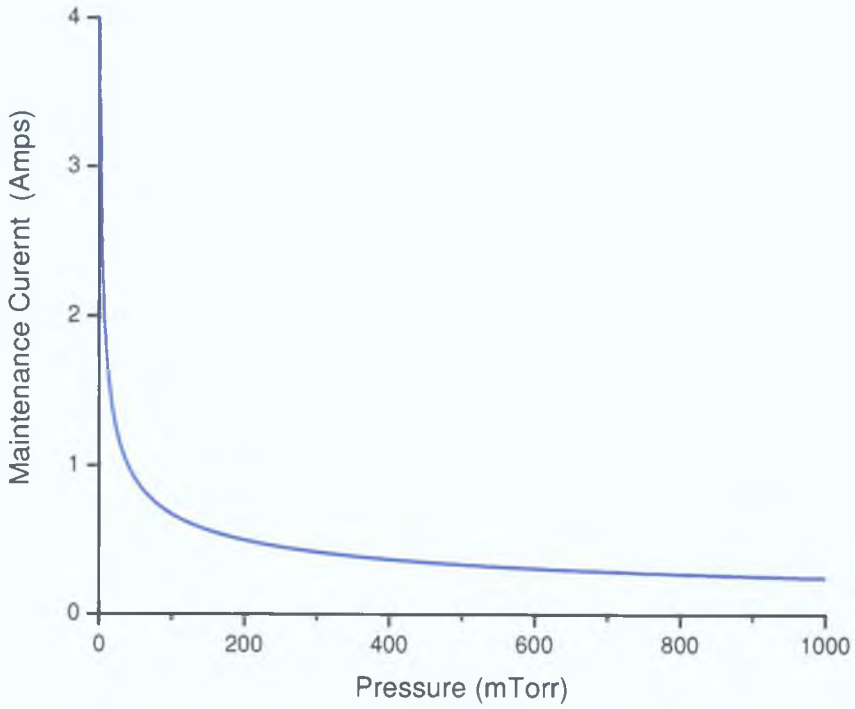

Figure 5.6: *Minimum maintenance current as a function of pressure*

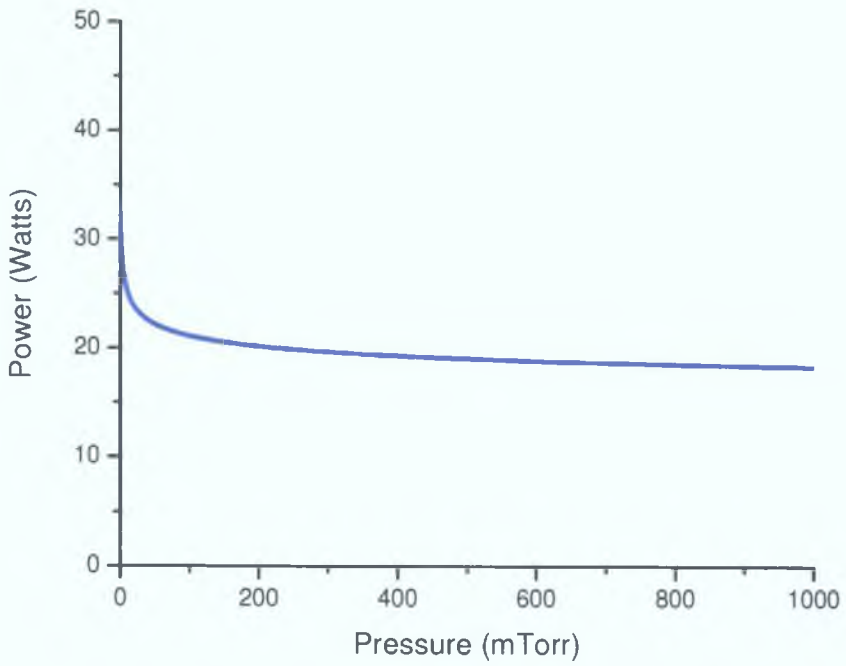

Figure 5.7: *Minimum maintenance power as a function of pressure*

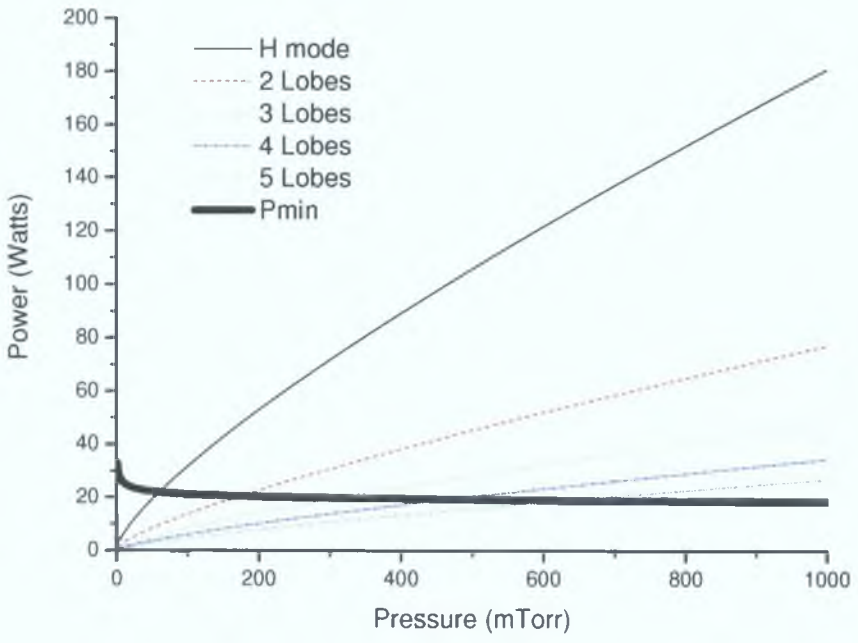

Figure 5.8: *Plasmoid Plot*

Overlaying figures 5.5 and 5.7 we see a plasmoid plot which defines the observable modes of plasmoids in an ICP as a function of pressure, and can be seen in detail in figure 5.9.

By comparing the theoretical (figure 5.11) and experimental (figure 5.10) plasmoid maps we see excellent qualitative agreement is shown for pressures in the collisional regime ($>$ 150 mTorr). The agreement is not as conclusive at lower pressure which is in the collisionless regime. At these low pressures, the much longer plasma diffusion length prohibits the formation of plasmoid lobes as plasma diffuses over a characteristic length greater than the inter plasmoid spacing.

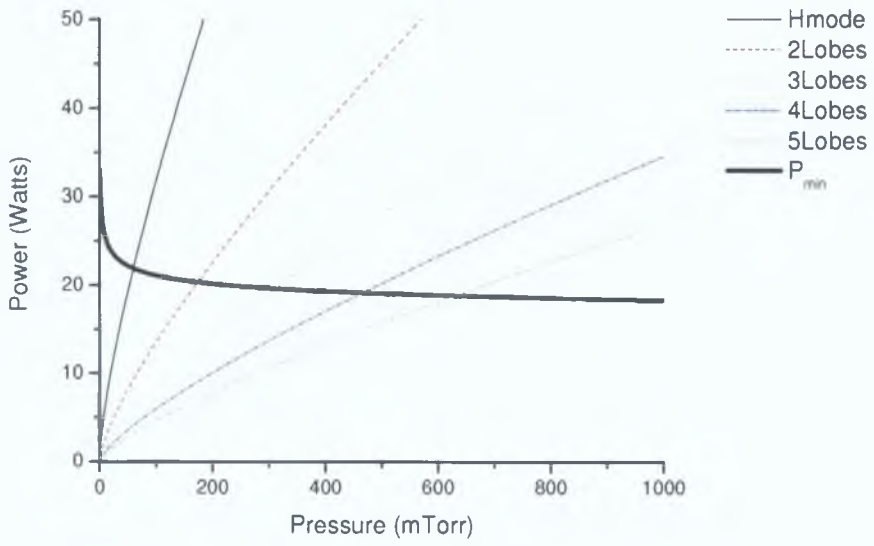

Figure 5.9: *Plasmoid Plot in detail*

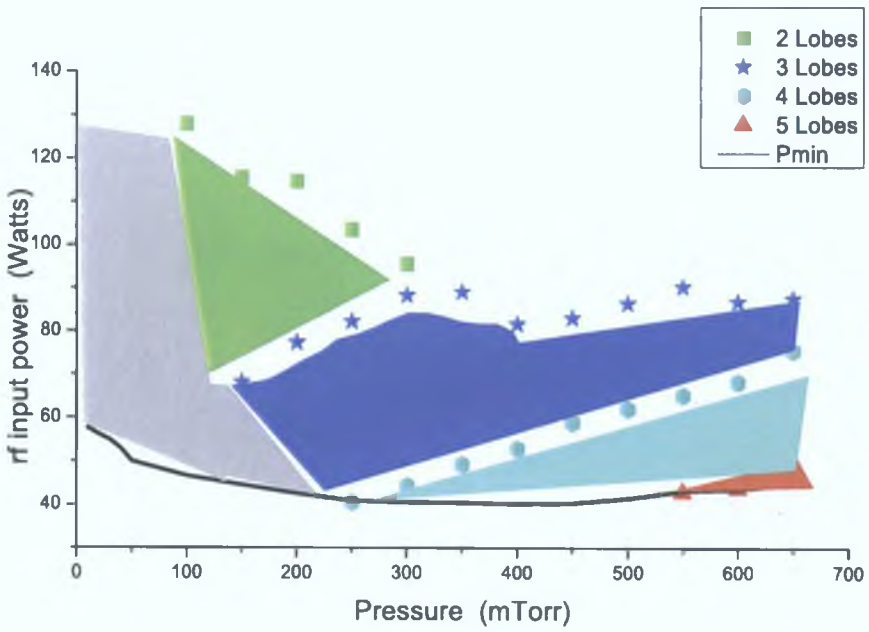

Figure 5.10: *Experimental Plasmoid Plot with the shaded areas illustrating the number of plasmoid lobes available in that region.*

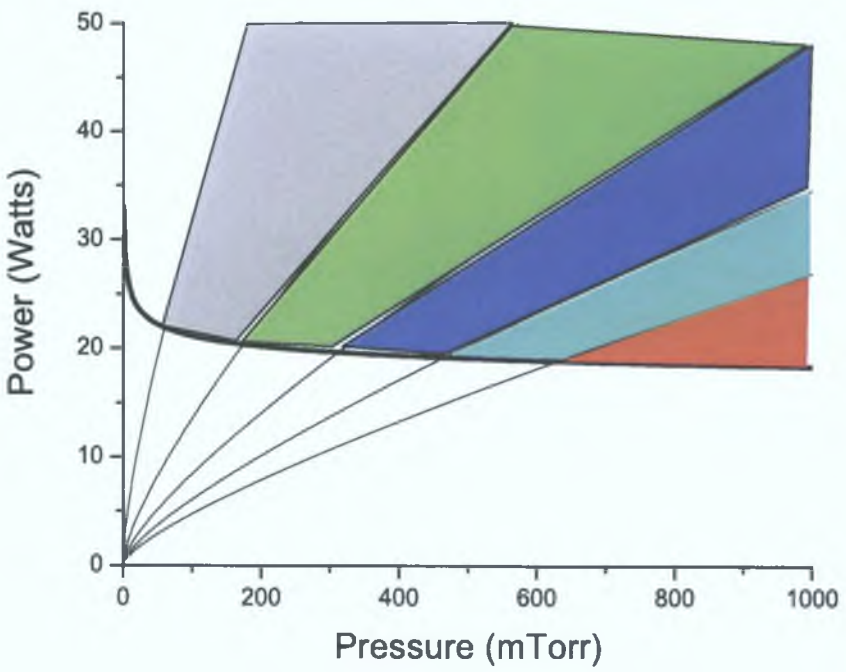

Figure 5.11: *Theoretical Plasmoid Plot with the shaded areas illustrating the number of plasmoid lobes available in that region.*

5.7 Diffusion length

The discussion above does not take into account possible diffusion of plasma particles between regions of high and low density Under certain circumstances this may inhibit the formation of plasmoids as described above due to the diffusion length of the plasma gradients at plasma densities and gas pressures being greater that the inter lobe distance of the plasmoids The diffusion of plasma from regions of high density to low density may prevent the formation of plasmoids as predicted by the discussion above In order to obtain a qualitative argument for the numbers of allowable plasmoid modes the diffusion length needs to be calculated for relevant parameter range of power and pressure

The plasma diffusion length is found by solving the diffusion equation for cylindrical geometry [27]

The faster more mobile electrons leave the plasma volume at a faster rate than the slower, heavier ions This leaves a charge imbalance with positive ions left inside the plasma while negative electrons escape A positive plasma potential is set up which retards the escape of electrons and enhances the escape of the ions The plasma potential adjusts until the fluxes of electrons and ions leaving the plasma are equal The flux, Γ, leaving the plasma is given by

$$\Gamma = \mu_i n\mathbf{E} - D_i \nabla n = \mu_e n\mathbf{E} - D_e \nabla n \tag{5 19}$$

where μ, n and $\mathbf{E}$ are the mobility, plasma density and electric field, respectively D is the diffusion coefficient with subscripts i and e referring to ions and electrons, respectively

Isolating $\mathbf{E}$ in equation 5 19 and substituting back into 5 19 for $\mathbf{E}$ give the expression for flux

$$\Gamma = \frac{\mu_i D_e + \mu_e D_i}{\mu_i + \mu_e} \nabla n \tag{5 20}$$

The ambipolar diffusion coefficient, D_a is given by

$$D_a \equiv \frac{\mu_i D_e + \mu_e D_i}{\mu_i + \mu_e} \tag{5 21}$$

The diffusion equation 5 22 relates the production of plasma with its production and loss terms

$$\frac{\partial n}{\partial t} = -D_a \nabla^2 n + \nu_{iz} n \tag{5 22}$$

where ν_{iz} is the ionisation frequency Assuming a steady state solution ($\frac{\partial n}{\partial t} = 0$) equation 5 22 becomes

$$\nabla^2 n - \left(\frac{\nu_{iz}}{D_a}\right) n = 0 \tag{5 23}$$

In cylindrical coordinates,$\nabla^2 n$ becomes

$$\nabla^2 n = \frac{\partial^2 n}{\partial r^2} + \frac{1}{r}\frac{\partial n}{\partial r} + \frac{1}{r^2}\frac{\partial^2 n}{\partial \theta^2} + \frac{\partial^2 n}{\partial z^2} \tag{5 24}$$

Assuming plasma uniformity in the axial and azimuthal directions, eliminates the θ and z components in (5 24) Substituting into (5 23) yields the Bessel equation

$$\frac{\partial^2 n}{\partial r^2} + \frac{1}{r}\frac{\partial n}{\partial r} + \left(\frac{\nu_{iz}}{D_a}\right) n = 0 \tag{5 25}$$

Which has the solution [27]

$$n = n_0 J_0 \left[\frac{r}{\Lambda}\right] \tag{5 26}$$

where the diffusion length,Λ, given by

$$\Lambda = \sqrt{\frac{D_a}{\nu_{iz}}} \tag{5 27}$$

The diffusion length determines the plasmoid mode available at any given pressure If the diffusion length Λ, is greater that the distance d, divided by the mode number n, then the mode must go into the next lowest mode available The mode number available for any given set of conditions is set by the inequality

$$\frac{d}{\Lambda} \leq n \tag{5 28}$$

The diffusion length as a function of pressure is plotted in Figure 5 12 Assuming an arbitrary skin depth of 8cm defining the plasma boundary, we obtain a distance d = $2\pi \times 8cm$ Plotting this distance divided by the diffusion length as a function of pressure (Figure 5 13) gives the number of allowable plasmoid lobes, mode number, for any given pressure

5.8 Summary

This plasmoid model details a theoretical explanation for the existence of plasmoids by considering the discharge to be an infinite transmission line exhibiting standing wave solutions of Mathieu's equation Plasma diffusion is introduced to give a lower limit to the observed number of plasmoids at a given pressure Although this theoretical explanation may explain plasmoid existence, it does not explain their formation from a uniform plasma The next chapter details this in a plasmoid simulation

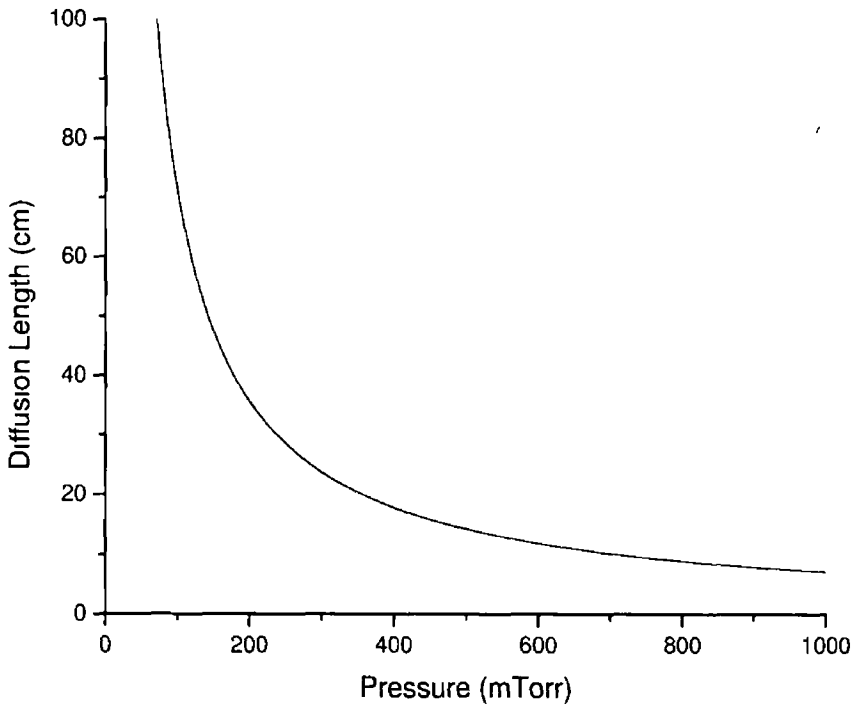

Figure 5 12 *Diffusion length as a function of Pressure*

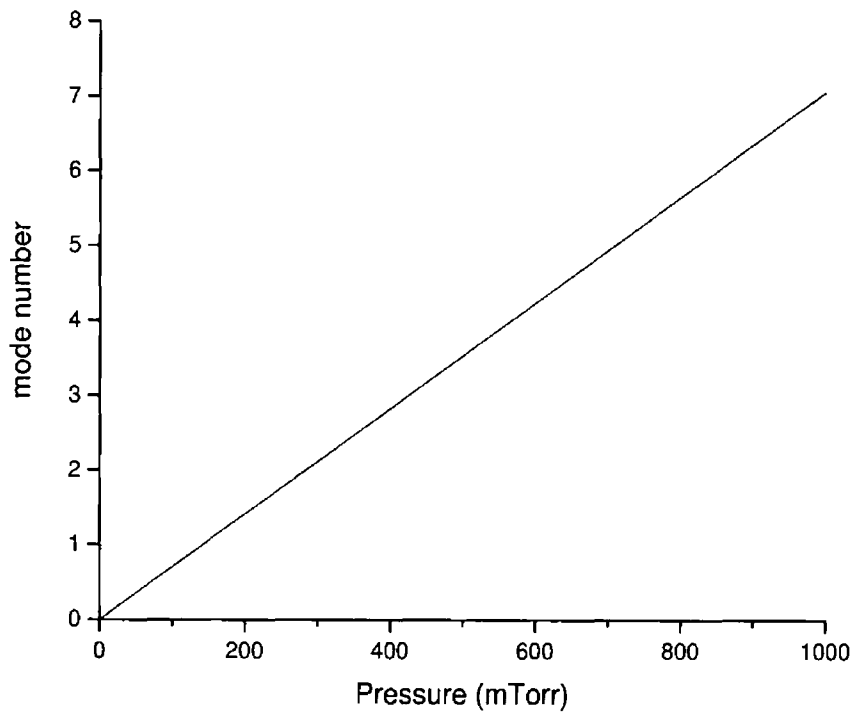

Figure 5 13 *mode number as a function of Pressure*

CHAPTER 6

Plasmoid Simulation

The previous chapter showed that plasmoids may form as standing wave solutions on an infinite transmission line These standing waves are stable solutions to Mathieu's equation In this chapter we couple the transmission line model to a model for local power absorption and simulate the time evolution of plasmoid formation in an inductively coupled plasma

The simulation describes an inductively coupled plasma at a particular power and pressure with a small density perturbation The density perturbation and the overall average density determine Mathieu 'a' and 'q' parameters The plasma current wave now travels along an infinite transmission line described by Mathieu's equation with parameters 'a' and 'q' As the plasma current travels around the current path, the plasma density grows or decreases depending on whether the average plasma density is in the inductive regime or in the capacitive regime (figure 6 1) At certain power and pressure ranges the plasma density is in the intermediate regime

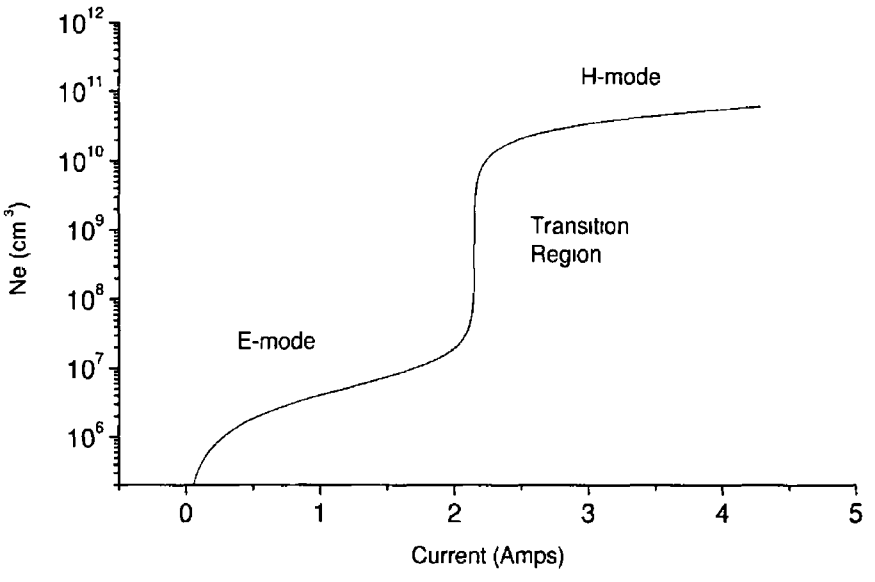

Figure 6 1 *Antenna Current as a function of electron density*

between capacitive and inductive coupling In this regime there is a sharp transition region between the capacitive and inductive modes in terms of plasma density In this region a small perturbation in plasma density can lead to a sharp increase in plasma current leading to a increase in plasma density This growth increases until the plasma density has reached the inductive region A small perturbation in the sharp transition region will be enhanced leading to a greater modulation of the spatial plasma density This causes the solutions of the Mathieu equation to be re-enforced leading to periodic solution where the peak density is generated via inductive coupling and the low density region is generated by capacitive coupling The division of power between the inductive and capacitive modes is a function of electron density The model for power absorption is based on the model used by Lieberman *et al* [17] for power absorption in an inductively coupled plasma including capacitive coupling The total power absorbed is $P_{abs} = P_{ind} + P_{cap}$ where P_{ind} and

P_{cap} are the inductive and capacitive power absorbed respectively [19]

6.1 Inductive Power

The inductive power absorbed varies linearly with electron density at low electron densities and varies as $n_e^{-1/2}$ at higher electron densities as the skin depth decreases the power deposition volume at higher densities The inductive power may be given as

$$P_{ind} = I_{rf}^2 R_{ind} \frac{n_e n_0}{n_e^2 + n_0^2} \frac{1}{V} \tag{6 1}$$

where I_{rf}, V and n_e are the antenna current, discharge volume and electron density respectively The value n_0 is the electron density value that corresponds to maximum power deposition We estimate this as the electron density value that corresponds to a skin depth $\simeq$ to the chamber radius Rearranging equation (5 8) we obtain

$$n_0 = \frac{2M_e \nu_{eff}}{\omega \mu_0 e^2 \delta^2} \tag{6 2}$$

where δ in this case $\simeq$ chamber radius Due to the complex nature of the power absorption circuit in discharge plasma ,R_{abs} is an arbitrary value chosen to obtain 'sensible' power values [19]

6.2 Capacitive Power

The capacitive power is given by

$$P_{cap} = I_{rf}^2 R_{abs} \frac{n_e}{n_e + n_c} \frac{1}{V} \tag{6 3}$$

where R_{abs} is as above and n_c is where the sheath thickness is comparable to the dielectric window thickness [19] We may obtain an estimate of the sheath thickness

using the matrix sheath approximation [13] Using Gauss' law in 1-D we obtain the standard relation

$$\frac{dE}{dx} = \frac{en_e}{\varepsilon_0} \tag{6 4}$$

and solving for the electric field, E, gives

$$E = \frac{en_e}{\varepsilon_0} x \tag{6 5}$$

and integrating E with respect to x we obtain the plasma potential

$$\Phi = -\frac{en_e}{\varepsilon_0}\frac{x^2}{2} \tag{6 6}$$

We obtain the sheath width, s, by rearranging equation(6 6) for the distance x, and setting Φ equal to the sheath voltage V_s

$$s = \left(\frac{2\varepsilon_0 V_s}{en_e}\right)^{\frac{1}{2}} \tag{6 7}$$

The sheath voltage, V_s may be obtained from the sheath potential at a floating wall [19] and is given by

$$V_s = -T_e Ln\left(\frac{M}{2\pi m}\right)^{\frac{1}{2}} \tag{6 8}$$

Rearranging equation (6 7) and setting it equal to the dielectric window thickness and inserting equation (6 8) allows us to obtain an estimate n_c

6.3 Power Loss

The power loss, P_{loss} , is given by

$$P_{diss} = n_e e u_B \epsilon_T A_{eff} \tag{6 9}$$

where u_B, A_{eff}, ϵ_T are the Bohm velocity, effective loss area, and the energy used to generate and electron-ion pair Balancing absorbed and lost power enables us to calculate the stable plasma operating density for a given value of antenna current (figure 6 2)

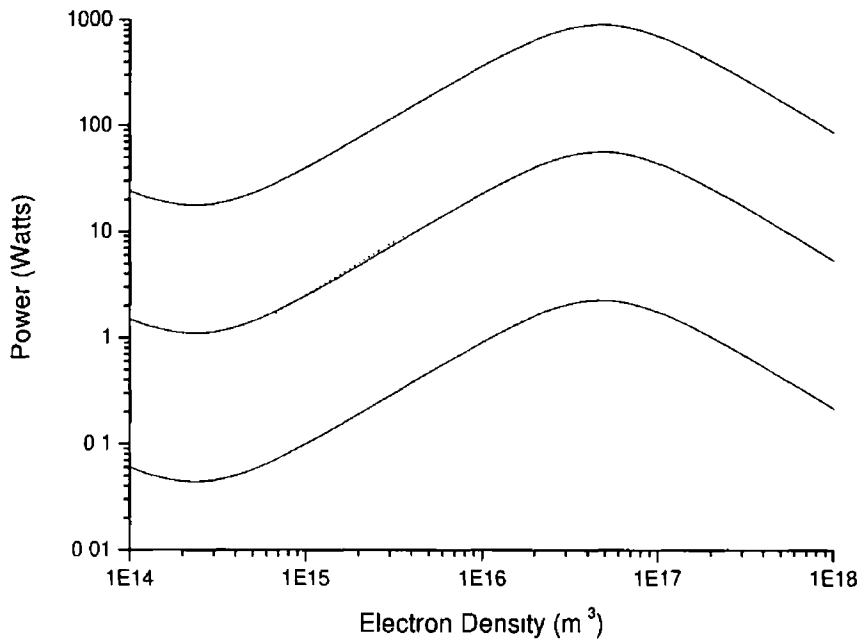

Figure 6 2 *Power absorbed and Power dissipated as a function of electron density The dashed curve represents the power dissipated, the solid curves represent the power absorbed for three antenna current values one in E-mode, one at maintenance current, and one in H-mode*

6.4 Diffusion

Diffusion is considered by adding a loss of electrons through the plasma sheath and considering spatial diffusion around the current path The electron particle balance fluid equation is used to describe the diffusion of electrons around the current path, volume ionisation and surface loss and the plasma sheath boundary[28] The 1-d electron particle balance equation is

$$\frac{\partial n_e}{\partial t} + \frac{\partial \Gamma_e}{\partial x} = n_e n_g K_{iz0} exp\left(\frac{-E_i}{kT_e}\right) \tag{6 10}$$

Where the right hand side of equation(6 10) is the volume ionisation term where n_e, n_g, K_{iz0}, E_i, T_e and k are the electron density, gas density, pre-exponential factor, ionisation energy, electron temperature and the bolztmann constant respectively Γ_e is the electron flux which for a 1-d plasma discharge is given by

$$\Gamma_e = -D_e \frac{dn_e}{dx} - n_e u_B \tag{6 11}$$

where D_e is the electron diffusion coefficient and u_B is the Bohm velocity Differentiating equation (6 11) we obtain

$$\frac{\partial \Gamma_e}{\partial x} = -D_e \frac{d^2 n_e}{dx^2} - \frac{n_e u_B}{dx} \tag{6 12}$$

Inserting into equation (6 10) we obtain the diffusion equation

$$\frac{\partial n_e}{\partial t} = n_e n_g K_{i0} exp\left(-\frac{Ei}{kT_e}\right) + D_e \frac{d^2 n_e}{dx^2} - \frac{n_e U_B}{dx} \tag{6 13}$$

6.5 Model Details

The model dynamics are solved in the following manner (figure 6 3) An initial spatial array containing 128 elements is created with an initial electron density and a small density perturbation A fourier transform is performed and the fundamental of the frequency spectrum is used to calculated the 'a' and 'q' parameters for equation

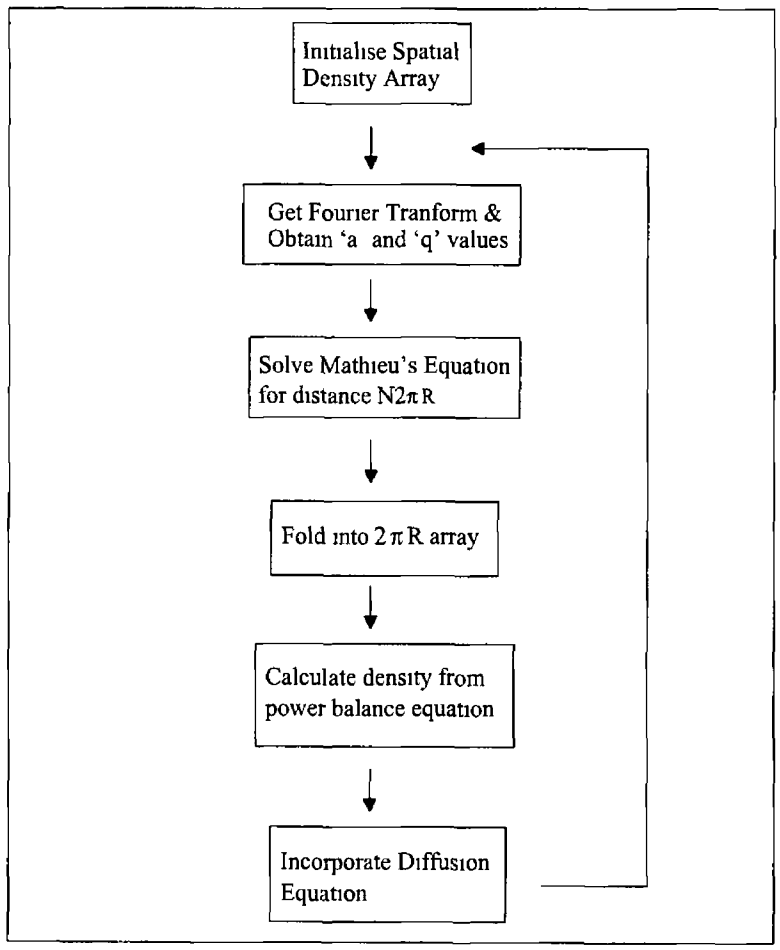

Figure 6 3 *Outline of the simulation process*

(5 1) Equation (5 1) is then solved over a distance z, corresponding to an integer number N, revolutions of the current path around the antenna This solution gives the plasma voltage variation over a distance $N2\pi R$ where R is the discharge radius This distance is then divided into N equal $2\pi R$ lengths which are then averaged to give the voltage for one current path The electron density corresponding to the local voltage is calculated using the power balance equation

The time evolution of the discharge is calculated using equation (6 13) which is discretised to the form

$$\Delta n_e = \left[n_e n_g K_{i0} exp\left(-\frac{E_i}{kT_e}\right) + D_e \left(\frac{n_{i+1} - 2n_i + n_{i-1}}{\Delta x^2}\right) - \frac{n_e U_B}{dx} \right] \Delta t \qquad (6\ 14)$$

The second term on the right hand side of equation (6 14) accounts for the diffusion of electrons around the plasma current path The subscript i corresponds to the element number of the array representing the current path and Δx is the element size The other terms are as previously outlined The procedure is repeated until a steady state is reached

6.6 Model Results

Figure 6 4 shows the formation of plasmoids lobes as a function of time for four different power and pressure values without consideration of plasma diffusion A steady state result of the plasmoid model is shown in figure 6 5 As can be seen the behaviour of the model corresponds qualitatively with the analytical solution to Mathieu's equation and experimental results (figure 6 6) However the depth of electron density modulation is two orders of magnitude which is greater than the experimental value of $\sim 1/2$ an order of magnitude as measured by Crowley

More plasmoid modes are available at higher pressure with the number of lobes decreasing with increasing power from the initial available mode number, consistent

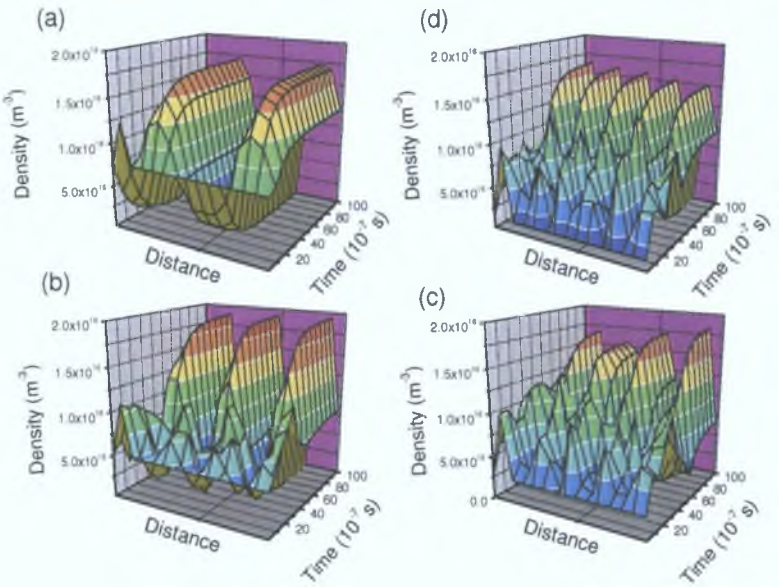

Figure 6.4: *Formation of plasmoids for a selection of Powers and Pressures: (a) 2 lobes at 100mTorr and 30 Watts (b) 3 lobes at 300mTorr and 20 Watts (c) 4 lobes at 500mTorr and 10 Watts (d) 5 lobes at 800mTorr and 5 Watts. The distance is the transmission line length for one revolution around the current path.*

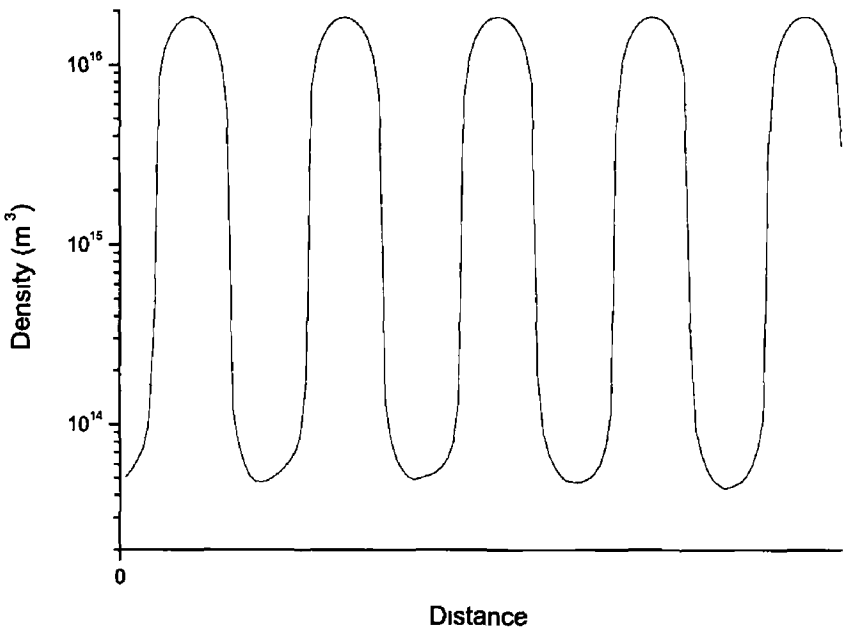

Figure 6 5 *Steady state plasmoids at 800mTorr and 5 Watts The distance is the transmission line length for one revolution around the current path*

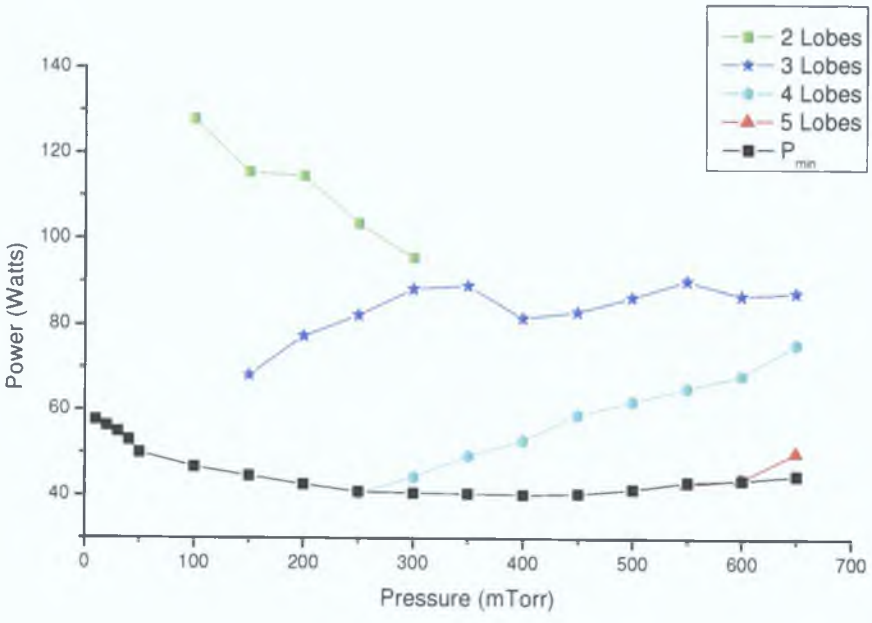

Figure 6.6: *Experimental plasmoid map showing up to 5 lobes.*

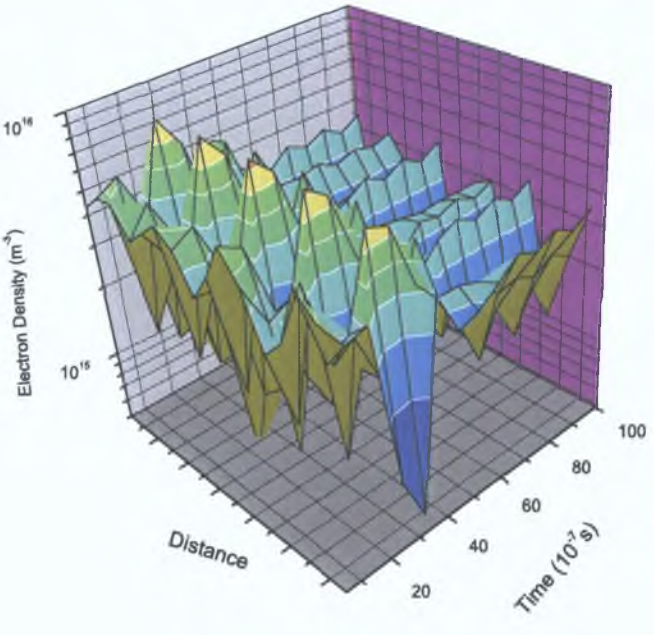

Figure 6.7: *Plasmoid simulation for pressure = 400mTorr and input power = 50 Watts including plasma diffusion. The distance is the transmission line length for one revolution around the current path.*

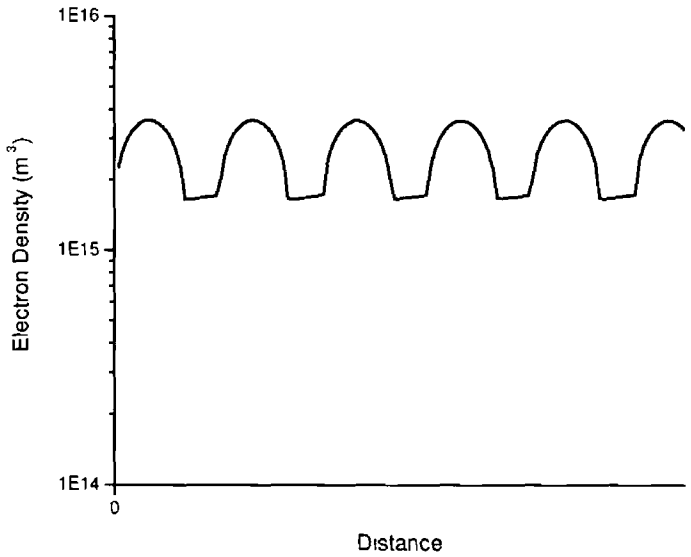

Figure 6 8 *Steady state solution showing the formation of plasmoid lobes at pressure = 400mTorr and input power = 50 watts including plasma diffusion. The distance is the transmission line length for one revolution around the current path*

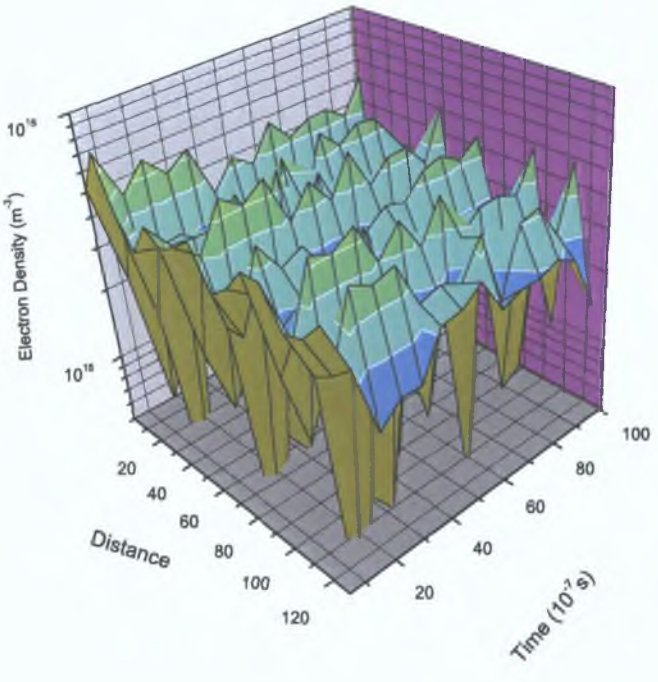

Figure 6.9: *Plasmoid simulation for pressure = 500mTorr and input power = 50 Watts including plasma diffusion. The distance is the transmission line length for one revolution around the current path.*

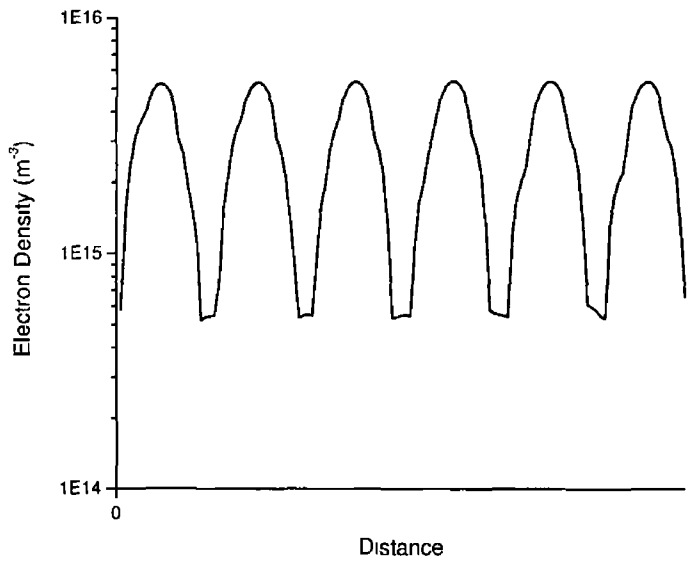

Figure 6 10 *Steady state solution showing the formation of plasmoid lobes at pressure = 500mTorr and input power = 50 watts including plasma diffusion The distance is the transmission line length for one revolution around the current path*

with observation Consideration of plasma diffusion as described above appears to give results more consistent results with experiment however model stability is reduced in doing so

6.7 Summary

The plasmoid simulation in this chapter is an extension of the theoretical model, and provides and explanation for plasmoid formation from a uniform plasma to one exhibiting plasmoids The primary mechanism at work is the division of power between capacitive and inductive coupling in a uniform plasma containing a small plasma density perturbation If the plasma is in the E-to-H instability window, a small density perturbation will cause a large change in plasma current which in-turn creates a larger density variation This amplification of the plasma density re-enforces the perturbation leading to the formation of stable standing waves observed as plasmoids and as illustrated by the plasmoid simulation

CHAPTER 7

Conclusions

Plasmoids are a gross spatial instability and are a widely observed phenomenon in radio-frequency discharges however, as yet, no generally accepted theory has been given to explain their formation

In this work, we observed that plasmoids occur in the E-to-H instability window and that their behaviour very much depends on the nature of this instability region We observed that for an ICP discharge containing pure argon, up to 4/5 plasmoids lobes could be obtained at moderately high pressures ($\sim$ 500-1000 mTorr), and exhibit rotation of a few hertz When small amounts (1-2 %) of molecular oxygen were added, the instability window increased in size giving a greater disparity between the E-to-H transition point and the H-to-E transition point This increase in the instability window dramatically affected the behaviour of the plasmoids as compared to the pure argon case The number of plasmoids obtainable was now much greater with up to 10 lobes observed The rotation rate also increased with

measured rotation rates as high as 60Hz With rotation rates as high as this, we were unable to resolve the number of lobes present and to the naked eye the plasma 'looked' uniform and stable, however a photomultiplier tube was able to detect light modulation at this frequency It is conceivable that under different plasma conditions, or in different ICP geometries, the mechanism responsible for plasmoids may give rise to higher frequency oscillations that are essentially plasmoid rotation at much higher frequencies

As yet, no generally accepted theory has been given to explain the formation of plasmoids We have proposed that plasmoids may be modelled as standing waves on an infinite transmission line as defined by the plasma In this treatment we have described the plasma as a transmission line with associated line capacitance and inductance This infinite transmission was modelled using Mathieu's equation which has characteristic standing wave solutions Using the plasma to define the transmission line, which is subsequently modelled using Mathieu's equation, gives qualitative agreement with the observed pressure dependency and antenna current dependency of the plasmoids The model predicts an increased number of lobes at higher pressure and a decrease in the number of lobes at higher antenna current A plasma diffusion length was calculated in order to obtain a lower pressure limit to plasmoid formation when the diffusion length becomes greater than the inter-plasmoid length thereby inhibiting plasmoid formation

As an additional 'check' of the theory, a simulation was run where an initially uniform plasma is given a density perturbation and allowed to evolve in time into a plasma with plasmoid lobes Again, the same pressure and antenna current dependency is observed and agrees with experimentally observed results

7.1 Suggestion for further work

- In order to gain further understanding of the E-to-H instability window, it would be useful to extend the simple argon global model to include excitation of argon atoms into excited states It is widely accepted that relatively long lived metastable argon atoms play a significant role in argon discharges Also, the extension of the global model to include argon/oxygen mixtures would also be useful

- Similarly, an extension of the transmission line model to include the effects of oxygen and other molecular gases in order to compare with experimental observations would further increase the understanding plasmoids

- The phenomenon of rotating waves similar to those found in [29] may be a useful extension of the time independent Mathieu equation A solution of a combination of radial and azimuthal standing waves leads to a rotating wave which could be applied to a plasma similar to the technique we have used This could give an explanation for plasmoid rotation

- Further experimental work in trying to observe instabilities in the instability window would give a useful insight into the physics behind the instability region Further work could be carried out using the phase resolved optical emission spectroscopy briefly described in the thesis A spatially resolved technique where the modulation of light inside and outside the plasmoid lobe could be measured could give interesting results

- Finally, Laser Induced Fluorescence (LIF) measurements of argon metastable atoms could give useful information to some ICP particle-in-cell (PIC) or Global Models that consider argon atom excitation

Bibliography

[1] M M Turner and M A Lieberman Hysteresis and the E-to-H transition in radiofrequency inductive discharges *Plasma Sources Sci Technol*, 8 313–324, 1999

[2] Brendan Crowley *An experimental investigation of heating mechanisms, mode transition and instabilities in a radio frequency inductively coupled discharge* PhD thesis, Dublin City University, 2000

[3] I M El-Fayoumi, I R Jones, and M M Turner Hysteresis in the E- to H-mode transition in a planar coil, inductively coupled RF argon discharge *J Phys D Appl Phys*, 31 3082–3094, 1998

[4] U Kortshagen, N D Gibson, and J E Lawler On the E-H mode transition in RF inductive discharges *J Phys D Appl Phys*, 29 1224–1236, 1996

[5] K Suzuki, K Nakamura, H Ohkubo, and H Sugai Power transfer efficiency and mode jump in an inductive RF discharge *Plasma Sources Sci Technol*, 7 13–20, 1998

[6] C S Corr, P G Steen, and W G Graham Instabilities in an inductively coupled oxygen plasma *Plasma Sources Sci Technol*, 12 265–272, 2003

[7] P Chabert, A J Lichtenberg, M A Lieberman, and A M Marakhtanov Instabilities in low-pressure electronegative inductive discharges *Plasma Sources Sci Technol*, 10 478–489, 2001

[8] R W Wood Plasmoidal high-frequency oscillatory discharges in "non-conducting" vacua *Phys Rev*, 35(7) 673–693, April 1930

[9] Finkelstein Ball lightning 135 A390A396, 1964

[10] Lawrence T Lamont and John J DeLeone Space charge instabilities in the rf induced gas discharge of the diode configuration *J Vac Sci Tech A*, 7(1) 155–158, 1969

[11] J Hopwood Review of inductively coupled plasmas for plasma processing *Plasma Sources Sci Technol*, 1 109–116, 1992

[12] G G Lister, Y-M Li, and V A Godyak Electrical conductivity in high-frequency plasmas *J Appl Phys*, 79(12) 8993–8997, June 1996

[13] Michael A Lieberman and Allan J Lichtenberg *Principles of Plasma Discharges and Materials Processing* Wiley, New York, 1994

[14] R B Piejak, V A Godyak, and B M Alexandrovich A simple analysis of an inductive rf discharge *Plasma Sources Sci Technol*, 1 179–186, 1992

[15] G Cunge, B Crowley, D Vender, and M M Turner Characterisation of the E to H transition in a pulsed icp discharge with internal coil geometry bi-stability and hysteresis *Plasma Sources Sci Technol*, 53 563–567, 1999

[16] G Cunge, B Crowley, D Vender, and M M Turner Characterisation of the E to H transition in a pulsed icp discharge with internal coil geometry bi-stability and hysteresis *Plasma Sources Sci Technol*, 53 563–567, 1999

[17] M A Lieberman, A J Lichtenberg, and A M Marakhtanov Instabilities in low pressure inductive discharges with attaching gases *Appl Phys Lett*, 75(23) 3617–3619, December 1999

[18] F Soberon Private communication, 2005

[19] Michael A Lieberman and Allan J Lichtenberg *Principles of Plasma Discharges and Materials Processing, second edition* Wiley, New York, 2005

[20] I M El-Fayoumi and I R Jones Theoretical and experimental investigations of the electromagnetic field within a planar coil, inductively coupled rf plasma source *Plasma Sources Sci Technol*, 7 162–178, 1998

[21] Rodney C Cross Demonstration of wave propogation in a periodic structure *Am J Phys*, 53 563–567, 1985

[22] Lawrence Ruby Applications of the mathieu equation *Am J Phys*, 64(1) 39–44, January 1996

[23] E L Mathieu Mémoire sur le mouvement vibratoire d'une membrane de forme elliptique *J Math Pures Appl*, 13 137–203, 1868

[24] P M Morse and H Feshbac *Methods of Theroetical Physics* McGraw-Hill, New York, 1953

[25] P Baille, Jen-Shih Chang, A Claude, R M Hobson, G L Ogram, and A W Yau Effective collision frequency of electrons in noble gases *J Phys B (Atom Molec Phys)*, 14 1485–1495, 1981

[26] J T Gudmundsson Magnetic induction and plasma impedance in a cylindrical inductive discharge *Plasma Sources Sci Technol*, 6 540–550, 1997

[27] V E Golant, A P Zhilinsky, and I E Sakha *Fundamentals of plasma physics* Wiley, New York, 1977

[28] David B Graves Fluid model simulations of a 13 56-mhz rf discharge Time and space dependence of rates of electron impact excitation *J Appl Phys*, 62(1) 88–94, July 1987

[29] Peter H Ceperley Rotating waves *Am J Phys*, 60 938–942, 1992